Variable Photon Energy Photoelectron Spectroscopic Study of CO Adsorption to Coordinatively Unsaturated Tetrahedral Cu(I) and Zn(II) Sites on CuCl(111) and ZnO(10$\bar{1}$0) Surfaces: d^{10} Contributions to CO Bonding and Activation

Jianyi Lin, Paul Jones, Jeff Guckert, and Edward I. Solomon*

Contribution from the Department of Chemistry, Stanford University, Stanford, California 94305.
Received March 26, 1991

Abstract: Cu is an intracrystalline promoter for methanol synthesis catalyzed by ZnO. High-affinity CO bonding to Cu/ZnO has been shown (Didziulis, S. V.; Butcher, K. D.; Cohen, S. L.; Solomon, E. I. *J. Am. Chem. Soc.* **1989**, *111*, 7110) to involve a coordinatively unsaturated tetrahedral Cu(I) site which is also present on the CuCl(111) model surface. CO is found to bind to the CuCl(111) surface nondissociatively with its molecular axis normal to the surface and with a high heat of adsorption of 23 ± 2 kcal/mol, similar to that of CO on Cu/ZnO. Variable photon energy photoelectron spectroscopy (PES) has been used to investigate the nature of this bonding and to compare this to CO bonding to the coordinatively unsaturated Zn(II) site on ZnO(10$\bar{1}$0). CO binding to CuCl is found to induce a shift of Cu $3d_\pi$ levels to deeper binding energy and to result in the presence of intense CO core level satellites, both results indicating the presence of π back-bonding of intermediate strength, which is not found to be present for CO bonding to ZnO. Differences in the σ bonding interaction are indicated by the 2.2 vs 1.3 eV shift of the CO 5σ peak to deeper binding energy upon adsorption on CuCl vs ZnO. This however is complicated by the CO 5σ interaction with the fully occupied Cu 3d band, which is found to be present from the 5σ photoemission cross section and shifts the 5σ peak energy but does not contribute to the net bonding interaction. A more direct probe of σ bonding is given by constant initial state (CIS) resonance PES studies at the metal $3p \rightarrow 4s$ transition edge which gives a 2.0 vs 0.8 eV shift in the M4s energy for CO adsorption on CuCl vs ZnO, demonstrating that σ bonding is stronger for CO/CuCl than CO/ZnO. This decrease in the σ and π bonding of CO to Zn(II) as compared to Cu(I) sites is ascribed to orbital contraction and d band energy stabilization associated with the higher effective nuclear charge on Zn(II). From He I PES work function studies the surface dipole moment is found to decrease and from NEXAFS studies the C-O bond length shortens upon CO adsorption to both d^{10} metal ion surfaces, demonstrating that in contrast to CO adsorption on transition-metal surfaces σ bonding plays a dominate role over π back-bonding for these two d^{10} ions. Analysis of XPS and Auger results shows the presence of positive effective atomic charge on the carbon end of the adsorbed CO molecule on both CuCl and ZnO. This positive charge on the carbon results from the dominance of σ donation and would activate the CO for nucleophilic attack by hydride. However the positive charge on carbon is found to be larger for Zn(II) than Cu(I), demonstrating that the additional promotional effect of Cu(I) is not electrostatic activation of CO but would appear to relate to the ability of Cu(I) to π back-bond which would stabilize later reaction intermediates in the catalytic mechanism of methanol synthesis.

I. Introduction

ZnO catalyzes methanol synthesis at high temperatures (573–673 K) and high pressures (150–200 atm) and is the active component in early industrial catalysts. The bonding of CO to ZnO has therefore been the subject of extensive surface science studies.[1-12] UPS studies on ZnO single-crystal surfaces have demonstrated that CO binds to coordinatively unsaturated tetrahedral Zn(II) ions on these surfaces, with a heat of adsorption of ~12 kcal/mol. The electronic structure of the CO molecule is not strongly perturbed by adsorption to the ZnO surface: its 4σ–1π splitting is found to be the same as that observed for gaseous CO, and the bonding shift to deeper binding energy of CO 5σ orbital is much smaller than the shifts observed for CO on metals. While CO adsorption studies have been reported for a wide variety of surfaces, ZnO surfaces are unusual in that a 1.2-eV decrease in the work function and a 59-cm^{-1} increase in the CO stretching frequency are observed upon CO adsorption. These changes are opposite to the behavior observed from CO chemisorption on metals and imply that the donation of charge from the CO 5σ orbital (which is weakly antibonding with respect to the CO bond) to ZnO dominates the bonding of CO to the surface Zn(II) ion.

The low-temperature (473–523 K), low-pressure (50–100 atm) commercial catalysts for methanol synthesis are Cu-promoted ZnO. These catalysts have a low activation barrier (18 vs 30 kcal/mol for pure ZnO)[13] and a high affinity CO binding site associated with the higher activity.[14] Therefore, CO adsorption studies have been extended to Cu/ZnO surfaces.[7,12] Our studies of the coordination chemistry of submonolayer coverages of copper on different ZnO single-crystal surfaces and their interaction with CO have determined that dispersed copper on the Zn-terminated (0001) and nonpolar (10$\bar{1}$0) surfaces is readily oxidized and annealed into the ZnO lattice as a Cu(I) site; this coordinatively unsaturated C_{3v} Cu(I) site is the only copper center found to adsorb CO with high affinity (21 kcal/mol). Dispersed atomic copper and copper clusters on the (0001) and (10$\bar{1}$0) surfaces chemisorb CO with approximately the same affinity as copper metal (15 kcal/mol), whereas the chemisorption of CO on dispersed Cu on the oxide-terminated ZnO(000$\bar{1}$) surface is even reduced from that on pure ZnO (<12 kcal/mol)[7]. Cu K-edge X-ray absorption spectroscopy (XAS) and extended X-ray absorption fine structure (EXAFS) studies[15,16] also reveal that Cu(I) sites are present in

(1) Gay, R. R.; Nodine, M. H.; Henrich, V. E.; Zeiger, H. J.; Solomon, E. I. *J. Am. Chem. Soc.* **1980**, *102*, 6752.
(2) D'Amico, K. L.; McClellen, M. R.; Sayers, M. J.; Gay, R. R.; McFeely, F. R.; Solomon, E. I. *J. Vac. Sci. Technol.* **1980**, *17*, 1080.
(3) Sayers, M. J.; McClellen, M. R.; Gay, R. R.; Solomon, E. I.; McFeely, F. R. *Chem. Phys. Lett.* **1980**, *75*, 575.
(4) McClellen, M. R.; Trenary, M.; Shinn, N. D.; Sayers, M. J.; D'amico, K. L.; Solomon, E. I.; McFeely, F. R. *J. Chem. Phys.* **1981**, *74*, 4726.
(5) D'Amico, K. L.; Trenary, M.; Shinn, N. D.; Solomon, E. I.; McFeely, F. R. *J. Am. Chem. Soc.* **1982**, *104*, 5102.
(6) D'Amico, K. L.; McFeely, F. R.; Solomon, E. I. *J. Am. Chem. Soc.* **1983**, *105*, 6380.
(7) Didziulis, S. V.; Butcher, K. D.; Cohen, S. L.; Solomon, E. I. *J. Am. Chem. Soc.* **1989**, *111*, 7110.
(8) Anderson, A. B.; Nichols, J. A. *J. Am. Chem. Soc.* **1986**, *108*, 1385.
(9) Campbell, C. T. In *Catalysis 1987*; Ward, J. W., Ed.; Elsevier: New York, 1988; p 783 and references therein.
(10) Au, C. T.; Hirsch, W.; Hirschwald, W. *Surf. Sci.* **1988**, *197*, 391.
(11) Fu, S. S.; Somorjai, G. A. *Surf. Sci.* **1990**, *237*, 87.
(12) Moretti, G.; Rossi, S. De.; Ferraris, G. *Appl. Surf. Sci.* **1990**, *45*, 341.
(13) Emmett, P. H. In *Catalysis Then and Now*; Franklin Publishing: Englewood, NJ, 1965.
(14) Klier, K. *Adv. Catal.* **1982**, *31*, 243 and references therein.
(15) Kau, L. S.; Hodgson, K. O.; Solomon, E. I. *J. Am. Chem. Soc.* **1989**, *111*, 7103; *J. Phys. (Paris)* **1986**, *C8*, 289.
(16) Sankar, G.; Vasudevan, S.; Rao, C. N. R. *J. Chem. Phys.* **1986**, *85*, 2291.

0002-7863/91/1513-8312$02.50/0

binary Cu/ZnO catalysts reduced in $CO/CO_2/H_2/N_2$ reaction mixtures. Since hydrogen activation through its heterolytic dissociation is known to proceed readily on ZnO, CO activation is likely involved in the rate-determining step and is promoted by the coordinatively unsaturated C_{3v} Cu(I) site which would thus appear to be the active center for the high activity methanol synthesis catalysts.[17]

In order to develop a detailed picture of CO bonding to a coordinatively unsaturated tetrahedral Cu(I) site, neither Cu/ZnO binary catalysts nor Cu-deposited ZnO single crystals are ideal in that these are not well defined pure systems. We have investigated CO adsorption on Cu_2O single-crystal surfaces;[18] however, this is also not an appropriate model system since Cu(I) cations are linearly coordinated to the oxide ions in the Cu_2O crystal. We have therefore focused on detailed spectroscopic studies of CO adsorption on pure CuCl(111) single-crystal surfaces. In CuCl crystals, copper and chlorine ions are combined in the zinc blende arrangement where each ion has four ions of the opposite type located at the corners of a regular tetrahedron and forming two interpenetrating face-centered cubic (fcc) sublattices. The zinc blende structure of CuCl produces three-coordinate unsaturated C_{3v} Cu(I) sites on the (111) surface, with a structure analogous to the Cu(I) site substituted for Zn(II) on the ZnO (0001) surface. The geometric and electronic structure of clean CuCl has been investigated using low energy electron diffraction (LEED), ultraviolet photoelectron spectroscopy (UPS), X-ray photoelectron spectroscopy (XPS), and variable photon energy photoelectron spectroscopy (PES).[19-23] No surface reconstruction has been observed from LEED studies of CuCl single-crystal surfaces.[19,20] The valence band PES spectrum of CuCl consists of a Cu 3d band and Cl 3p band, which are well-separated and centered at about 2 and 6 eV below the Fermi level, respectively. The empty Cu 4s level is observed, by resonance PES, at about 2.5 eV above the Fermi level.[22] The electronic structure of CuCl is not significantly different from that of Cu_2O (i.e. the copper(I) chloride and oxide σ and π donations to bonding are found to be quite similar) but is very different from that of ZnO. In ZnO, the metal 3d band is centered at 10.7 eV relative to the Fermi level, well below the O 2p level (between 4 and 8 eV below the Fermi level), and the empty 4s level is situated at 0.4 eV above the Fermi level. These significant differences in d^{10} electronic structure are expected to result in different bonding descriptions for CO/CuCl and CO/ZnO, which should contribute to differences in catalysis. To date, no study of CO adsorption on CuCl surfaces has been reported, although CuCl has been known for over a century to strongly interact with CO, and CuCl ammonia complex solutions are widely recognized as the best means for quantitatively absorbing CO under mild conditions.

The principal technique used in this study is PES. Similar to our earlier studies of CO on ZnO,[1,3] the angular dependence of the He II UPS spectrum was measured in order to determine the molecular orientation of the adsorbed CO molecule and to assign the energies of the chemisorbed CO valence orbitals: 4σ, 1π, and 5σ, which correspond to the oxygen lone pair, the π bond, and the carbon lone pair, respectively. At a photon energy of 40.8 eV (He II resonance), the CO 4σ and Cu 3d cross sections are large and only a low background of secondary electrons is observed in the valence band region. This allows heat of adsorption measurements to be made by monitoring intensity changes of the CO 4σ peak as a function of surface temperature and CO gas pressure. He I UPS is used mainly to measure the work function and the band bending changes in order to determine the surface dipole moment change due to CO adsorption. All these experiments use resonance excitation sources and parallel our previous PES studies on the CO/ZnO system. These results are presented and analyzed in section IIIA. Section IIIB presents the results of CO/CuCl(111) studies with synchrontron radiation. The high degree of polarization and tunability of synchrotron radiation enable one to perform (1) variable photon energy PES, (2) constant initial state (CIS)[24,25] and resonance PES, (3) core-level photoemission and corresponding Auger electron spectroscopy, and (4) near edge X-ray absorption fine structure (NEXAFS) studies. By utilizing these techniques, (1) the photon energy dependence of CO-induced PES peaks has been analyzed to obtain information on covalent bonding; (2) the unoccupied Cu 4s state and its shift upon CO adsorption has been determined; (3) the shake-up satellite of the C 1s level has been observed and analyzed, and the energy positions of the C 1s level and the C KVV Auger lines have been determined, which provide information on the effective charge on the carbon end of the adsorbed CO; and (4) the C–O bond length for the adsorbed CO on the CuCl surface has been obtained. For comparison we have also extended our earlier study of CO on ZnO($10\bar{1}0$) to include these synchrotron radiation experiments. These results are presented in section IIIC. On the basis of the results and analyses in section III, we can evaluate differences in CO bonding and activation by Cu(I) and Zn(II) d^{10} ions, which is discussed in section IV.

II. Experimental Section

CuCl(111) surfaces were prepared by cutting a 1-mm plate from a single crystal of CuCl, and the orientation was checked to within ±1° by Laue backscattering. The surface was then polished with alumina grit down to 0.1 μm until no pits were visible and chemically etched with a mixture of concentrated hydrochloride and anhydrous ethanol followed by an acetone rinse. Surface cleaning was completed in UHV by a series of sputter/anneal cycles. Because CuCl is a binary semiconductor with a low melting point, care was taken in preparing a clean, reproducible surface by ion sputtering. At energies higher than 1.1 keV this resulted in the preferential loss of chlorine; therefore, argon ion sputtering was performed at energies between 900 and 1000 eV with an ion flux density of 1–4 mA/cm^2. Annealing compensated for any loss of chlorine during sputtering. The sample temperature was maintained at approximately 350 K throughout the sputter and anneal process.

The surface cleanliness, chemical stoichiometry, and metal oxidation state were monitored with XPS and UPS. Electron beam induced Auger spectroscopy was not used in the study of CuCl due to the high probability of surface damage from the electron beam, as was observed in our scanning Auger microscope experiments. A clean surface produced XPS spectra with no photoemission features other than those of Cu and Cl. The atomic ratio of copper vs chlorine was estimated from the intensities of the Cu $2p_{3/2}$ and Cl 2p bands based on the formula given in ref 26. Since the Cu 2p level lies at the same binding energy for both Cu(I) and Cu(0), the oxidation state of copper was determined by using the X-ray-induced Cu $L_3M_{4,5}M_{4,5}$ Auger peak. Prolonged X-ray irradiation at room temperatures was found to result in changes in the Cu/Cl atomic ratio[19,27] and was therefore avoided.

The surface order was checked by LEED, which showed a hexagonal pattern for the clean surface, indicating that no symmetry changing surface reconstruction occurs. LEED patterns were observed only when the energy of the incident electron beam was higher than a threshold value, which is the secondary emission crossover.[28,29] For CuCl this is

(17) It should be noted that there is some controversy on the role of CO_2 in methanol synthesis from syngas. Some experiments including isotope labeling have suggested that CO_2 is the main source of carbon for methanol (in particular, at low conversions) (Chinchen, G. C.; et al. *Appl. Catal.* **1987**, *30*, 333; **1988**, *36*, 1. Bowker, M.; et al. *J. Catal.* **1988**, *109*, 263. Waugh, K. C. *Catal. Lett.* **1990**, *7*, 345). Alternatively other researchers have determined that the role of CO_2 is to maintain the Cu(I) species on catalyst surfaces, which are thought to be active centers for the CO conversion to methanol (refs 14 and 12; Apai, G. R. *J. Chem. Soc., Chem. Commun.* **1984**, 212).

(18) Lin, J.; Solomon, E. I. To be published.

(19) Kono, S.; Ishii, T.; Sagawa, T.; Kobayasi, T. *Phys. Rev. B* **1973**, *8*, 795.

(20) Westphal, D.; Goldmann, A. *J. Phys. C: Solid State Phys.* **1982**, *15*, 6661; *Solid State Commun.* **1980**, *35*, 441.

(21) Ishii, T.; Taniguchi, M.; Kakizaki, A.; Naito, K.; Sugawara, H.; Nagakura, I. *Phys. Rev. B* **1986**, *33*, 5664.

(22) Didziulis, S. V.; Cohen, S. L.; Gewirth, A. A.; Solomon, E. I. *J. Am. Chem. Soc.* **1988**, *110*, 250.

(23) Didziulis, S. V.; Cohen, S. L.; Butcher, K. D.; Solomon, E. I. *Inorg. Chem.* **1988**, *27*, 2238.

(24) Lindau, I.; Spicer, W. E. In *Synchrotron Radiation Research*; Winick, H., Doniach, S., Eds.; Plenum Press: New York, 1980; p 159.

(25) Kunz, C. In *Photoemission in Solids*; Ley, L., Cardona, M., Eds.; Wiley: New York, 1978; Vol. II, p 299.

(26) Wagner, C. D.; Riggs, W. M.; Davis, L. E.; Moulder, J. F.; Mullenberg, G. E. In *Handbook of X-ray Photoemission Spectroscopy*; Perkin-Elmer, 1979; p 28.

(27) Sesselmann, W.; Chuang, T. J. *Surf. Sci.* **1986**, *176*, 67.

(28) French, T. M.; Somorjai, G. A. *J. Phys. Chem.* **1970**, *74*, 2489.

dependent on the CO surface coverage as well as the sample temperature and incident beam current, and therefore it also served as an indicator of adsorption.

ZnO samples were also 1-mm-thick single-crystal plates. The sample was oriented within 1° of the (10$\bar{1}$0) direction by Laue backscattering and polished with alumina grit and etched with a 5% HCl solution. Ar ion sputtering was performed successively at accelerating potentials of 1000, 500, and 250 V at 720 K in UHV, followed by annealing at these temperatures. ZnO sample cleanliness was checked with Auger spectroscopy.

All experiments utilizing resonance photon sources were carried out in a Vacuum Generators ESCALAB MK II instrument equipped with XPS, UPS, AES, and LEED capabilities. Of the two sources available with the twin-anode X-ray probe, the Mg Kα (1253.6 eV) was normally used due to its higher resolution. A discharge lamp produced He II (40.8 eV) and He I (21.2 eV) photons propagating at an angle 15° off the vertical. The hemispherical electron energy analyzer (150° spherical sector of 150-mm radius) with a small 6° cone of acceptance in one direction and 90° in the other direction allowed angular dependent photoemission studies by rotating the single-crystal surface relative to the incident beam.[29] The sample was heated and cooled in situ; the sample temperature was measured with use of a chromel–alumel thermocouple attached to the sample holder.

All gases used were of research purity (Matheson, 99.99%). CO was introduced into the experimental chamber from a separate UHV line through a Varian leak valve. Carbon monoxide pressure and doses were monitored with an ionization gauge. The base pressure of the system was maintained at $\sim 5 \times 10^{-11}$ mbar (2×10^{-10} mbar with the He resonance lamp in operation). All adsorption experiments were carried out at low temperatures. CuCl is a p-type semiconductor with a wide band gap of 3.4 eV.[30] At low temperatures charging caused by photoemission became severe due to rather poor conductivity of the sample. An electron flood gun was therefore employed (operated at 1.5–2.0 V and 2.0 A) in order to compensate for this charging without distorting the overall spectral shape. Nevertheless, some sample charging would occur, and this was taken into account by using the Cl 2p core and Cl 3p valence levels as references.

Experiments employing synchrotron radiation were primarily performed on SPEAR beam line III-1 at the Stanford Synchrotron Radiation Laboratory (SSRL) under dedicated conditions with a grasshopper monochromator. Variable inlet and exit slits on the monochromator allowed an energy resolution of 0.2 eV to be maintained for most photon energies. The UHV system used for these experiments was a Perkin-Elmer PHI chamber with a double-pass cylindrical mirror analyzer (CMA), electron flood gun, and ion sputtering gun. The CMA accepts a 6° cone of electrons with a half angle of 42.5° off the CMA axis. For UPS studies a narrow analyzer slit and a small pass energy (25 eV) were chosen for the CMA, resulting in a constant instrument resolution of 0.2 eV, whereas for NEXAFS measurements and core level PES, wider analyzer slits and larger pass energies were utilized to increase the signal-to-noise ratio. The incident synchrotron radiation was fixed at an angle of approximately 75° with respect to the central axis of the CMA and impinged on the sample at a small angle close to the grazing. Spectra were normalized to the incident photon flux which was monitored by collecting the total electron yield from a high-transmission nickel mesh freshly coated with gold in UHV. All spectra were signal-averaged until a satisfactory signal-to-noise ratio had been established. As the SSRL experiments could not be performed in an ambient of CO, adsorption was obtained by saturating the surface, which was accomplished at 80 K by a 15-min exposure to 1×10^{-5} mbar of CO. This was followed by evacuation of the chamber and taking PES data. Loss of the CO surface coverage with time was monitored by using the CO 4σ peak intensity ($h\nu$ = 40 eV) at regular time intervals throughout data collection. If the CO peak intensity appeared to be significantly reduced, the sample was reexposed to CO as described above.

Constant initial state (CIS) spectra were obtained at the metal 3p → 4s edges. The photoelectron kinetic energy and the photon energy were simultaneously scanned through the metal 3p absorption edge. The constant initial state was set at the metal 3d satellite maximum. Constant final state (CFS) spectroscopy was employed to obtain near edge X-ray absorption fine structure (NEXAFS) data on the C 1s level of chemisorbed CO. To increase surface sensitivity, the carbon KLL Auger electrons with kinetic energy of 265–270 eV were detected as a function of photon energy.

NEXAFS experiments for CO/CuCl(111) were also performed at the National Synchrotron Light Source (NSLS) at Brookhaven National Laboratories. A plane grating grazing monochromator was utilized to provide a tunable photon beam with an energy resolution of 0.2 eV maintained for all photon energies. A Vacuum Generators UHV system, equipped with a double-pass CMA and electron flood gun, was employed. The incident synchrotron radiation was fixed at an angle of 88° with respect to the central axis of the CMA. By rotating the CuCl sample, NEXAFS data were obtained at two different incidence-detection geometries: incidence angles of 19° and 47° off the surface normal, corresponding to spectra polarized with the A vector of light approximately perpendicular to and 43° off the surface normal, respectively. Exposing the sample at 130 K to 1×10^{-5} mbar of CO gas for 15 min produced a CO-saturated surface that did not change significantly during data collection.

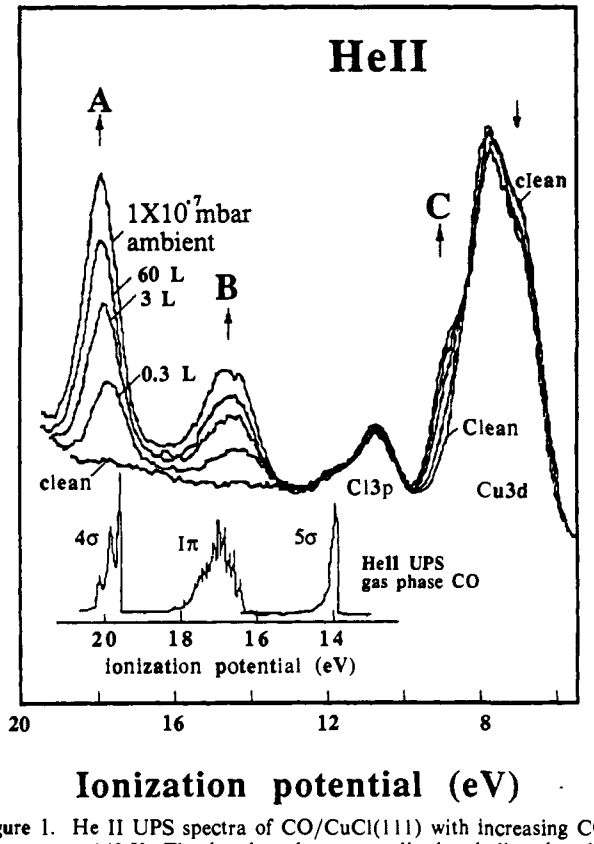

Figure 1. He II UPS spectra of CO/CuCl(111) with increasing CO converage at 140 K. The data have been normalized and aligned to the least-perturbed Cl 3p band. Peaks A, B, and C grow with increasing CO coverage, while the intensity of the Cu 3d band decreases as indicated by arrows. The He II UPS spectrum of gas-phase CO taken from ref 32 is included at the bottom with its 4σ peak aligned to peak A. This alignment is achieved by shifting the CO gas-phase spectrum to lower binding energy by 1.7 eV.

III. Results and Analysis

A. He I and He II UPS Studies of CO/CuCl(111). 1. Photoemission Spectra and Their Angular Dependence. Once the CuCl sample had been characterized by XPS and LEED, He I and He II photoelectron spectra of the clean surface were collected at 140 K. From Figure 1, the He II valence band spectrum of the clean CuCl(111) surface consists of two major features: a Cu 3d band centered at 7 eV and a Cl 3p band at 11 eV below the vacuum level.[31] Both the Cu 3d and Cl 3p bands consist of two peaks, with features at 6.9, 7.9, 10.7, and 12.0 eV relative to the vacuum level, in agreement with previously reported PES spectra of polycrystalline CuCl.[22,23] Exposing the surface to CO at low temperature results in two additional peaks at 18.0 and 14.7 eV below the vacuum level (A and B in Figure 1). The intensity of

(29) Fuggle, J. C.; Steinkilberg, M.; Menzel, D. *Chem. Phys.* **1975**, *11*, 307.

(30) Nikitine, S. *Prog. Semicond.* **1962**, *6*, 271.

(31) The energy levels reported here for the CuCl surfaces are all referenced to the vacuum level, rather than to the Fermi level, because at low temperatures, the conductivity of CuCl is rather poor, and charging and band bending changes can complicate the determination of the Fermi level.

(32) Schweig, A.; Thiel, W. *J. Electron Spectrosc. Relat. Phenom.* **1974**, *3*, 27.

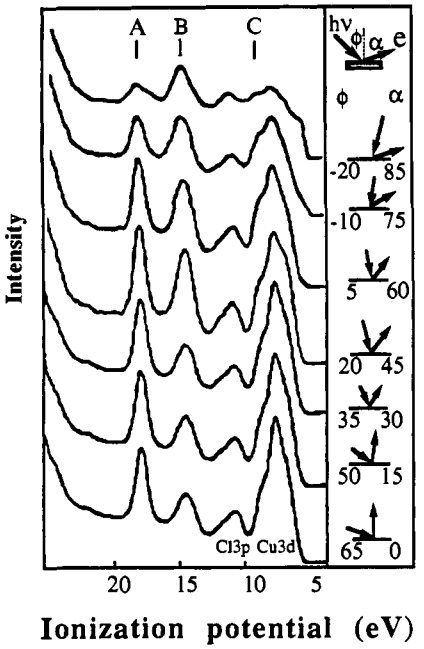

Figure 2. Angular dependence of He II UPS spectra of CuCl(111) in a CO ambience of 1×10^{-7} mbar at 140 K. The spectra were obtained at different incidence (ϕ)–detection (α) geometries which are described to the right of each spectrum.

peaks A and B grows with increasing CO coverage until saturation is reached. In Figure 1 the He II UPS spectra at different CO exposures are aligned and normalized with respect to the least-perturbed Cl 3p band. A small successive shift of the CO-induced peaks A and B to deeper binding energy is observed with increasing coverages up to saturation. This shift is a general feature of CO adsorption and has been attributed to a change in relaxation associated with higher coverages.[33,34]

In addition to the new peaks A and B, Figure 1 also shows a significant change in the Cu 3d band region due to CO adsorption. The 3d peak is attenuated and a high-energy shoulder (peak C in Figure 1) appears at the deep-binding energy side of the Cu 3d band. The intensity of this shoulder increases with increasing CO coverage.

The angular-dependent He II UPS spectra for CO/CuCl(111) at 140 K with an ambient CO pressure of 1×10^{-7} mbar are presented in Figure 2. The light source used in these experiments is unpolarized. As shown to the right in these figures, the angle (relative to the surface normal) of light incidence, ϕ, and the angle of photoelectron collection, α, vary, while the angle between the incident light and detected photoelectrons remains fixed at 65°. On going from the bottom to the top spectrum in Figure 2 the photoelectron collection angle increases from 0° to 85° with respect to the surface normal, while the intensity of peak A relative to peak B successively decreases.

Davenport's calculations[35] have indicated that the σ states should couple to $A_{\parallel}$ (the component of the light parallel to the molecular axis) and emit photoelectrons mostly at the direction parallel to the molecular axis, while a π state should couple to $A_{\perp}$ (the component of the light perpendicular to the molecular axis) and have maximum photoelectron emission at large angles off the molecular axis. This dipole selection rule can also be applied to unpolarized light by adding the contributions from the two polarizations, as has been confirmed by Horn et al.[34]

On a CuCl(111) surface, the coordinatively unsaturated Cu(I) sites have C_{3v} symmetry with open coordination positions parallel to the surface normal. According to the dipole selection rules given above, if an adsorbed CO molecule is bound to a surface copper site along the unsaturated direction, one would detect CO 4σ and

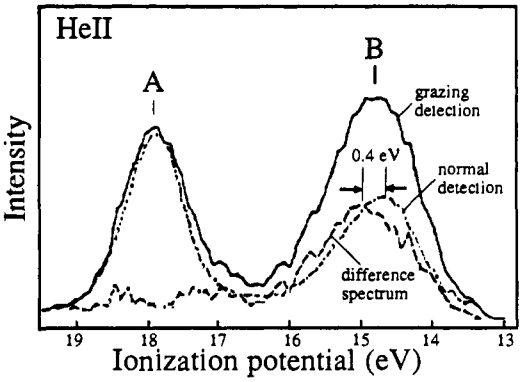

Figure 3. Comparison of He II UPS spectra of CO/CuCl(111) at different photoelectron detection angles. The solid line is for grazing (large detection angle off the surface normal) detection and the dash-dot line for normal detection. These two spectra are aligned and normalized with respect to peak A. The broken line is the difference spectrum, which is found to shift to deeper binding energy relative to peak B in normal detection by 0.4 eV.

5σ states most strongly in the direction parallel to the surface normal. Alternatively, the CO 1π state should show maximum emission intensity at large angles off the surface normal. Peak A in Figure 2 has the highest ionization potential of the CO-derived valence molecular states. This peak has maximum intensity in the bottom spectrum where the A vector of the incident beam, which is perpendicular to the direction of propagation, is normal to the surface, and photoelectron detection is along the surface normal. Therefore, peak A must originate from a σ level and can be assigned as the CO 4σ photoemission peak. Alternatively the relative intensity of peak B is weak at normal emission (bottom spectrum in Figure 2) and reaches a maximum at the largest collection angle (top spectrum). Thus peak B exhibits π symmetry and must contain photoemission from the CO 1π orbital. The fact that the intensity ratio of the 1π peak relative to the 4σ peak reaches a maximum in the top spectrum, for which photoelectrons were collected at nearly a right angle off the surface normal, confirms that the adsorbed CO must be bound to the CuCl(111) surface with the C–O bond axis perpendicular to the surface. The deviation of the CO orientation off the surface normal is estimated to be less than 10°, as seen from the top two spectra in Figure 2.

An energy splitting of 3.3 eV is observed between peaks A and B, 0.5 eV larger than the 2.8-eV splitting observed between the 4σ and 1π levels in gaseous CO (included in Figure 1). Since neither the 4σ nor the 1π orbitals are directly involved in CO bonding to the CuCl surface, this deviation from the gas-phase value is unlikely to be caused by an initial state shift of the 1π level relative to the 4σ level.[36] Consequently, peak B could be a composite peak consisting of contributions from both the CO 1π and 5σ orbitals, the latter not being observed to lower binding energy in the CO/CuCl spectrum. The CO 5σ level is directly involved in metal–CO bonding and should be shifted significantly to deeper binding energy, relative to the 5.7-eV 4σ–5σ splitting in gas-phase CO (Figure 1, bottom).

Figure 3 compares the top and bottom He II UPS spectra from Figure 2 (detector at grazing angle (π enhanced) and nearly normal (σ enhanced) to the surface), which have been aligned and normalized with respect to the 4σ peak (peak A) to compensate for σ intensity variation with angle. In addition to the significant enhancement in intensity of peak B with grazing angle detection, the peak maximum has shifted to higher binding energy. This change in energy with angle reveals that two transitions contribute to peak B. Thus the 5σ must overlap with the 1π contribution. The difference between the two spectra is also included in Figure 3 and exhibits a displacement of the peak B centroid to 0.4 eV deeper binding energy relative to the normal

(33) Gay, R. R. Ph.D. Thesis, MIT, 1979.
(34) Horn, K.; Bradshaw, A. M.; Jacobi, K. *Surf. Sci.* **1978**, *72*, 719.
(35) Davenport, J. W. Ph.D. Thesis, University of Pennsylvania, 1976.
(36) Rhodin, T. N.; Tsai, M.; Kasowski, R. V. *Appl. Surf. Sci.* **1985**, *22/23*, 426 and references therein.

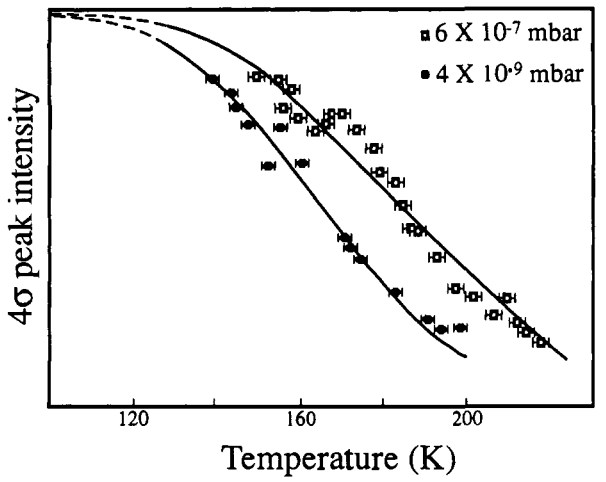

Figure 4. Variation of the CO 4σ peak intensity of CO/CuCl(111) as a function of temperature for CO ambient pressures of 4×10^{-9} and 6×10^{-7} mbar. Solid lines fit the surface coverage as a function of temperature using $\theta/(1-\theta) = K \cdot P \cdot \exp[\Delta H_0(1-\alpha\theta)/RT]$ (see ref 33) with $\alpha \simeq 0.6$ and $K \simeq 7.8 \times 10^{-14}$ for $P = 6 \times 10^{-7}$ mbar.

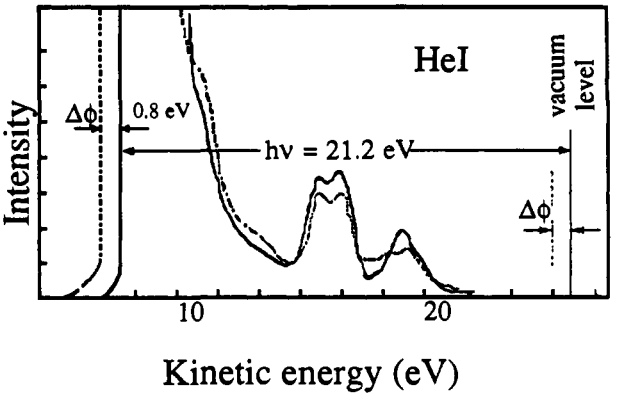

Figure 5. He I PES study of the work function change of CuCl upon CO adsorption. The solid line is the He I UPS spectrum for the clean CuCl(111) surface, while the broken line is for the CO-saturated surface at 140 K and 1×10^{-7} mbar of CO ambient. The spectra are aligned to the Cl 3p band to correct for changes in band bending. Note that the scale used here is KE, not IP = 21.2 − KE. The 0.8-eV shift to lower kinetic energy in the onset of the secondary electron tail thus corresponds to the surface dipole moment change upon CO adsorption.

detection spectrum. Since the intensity of peak B in the difference spectrum arises primarily from a π symmetry state, the CO 1π component of peak B must lie to deeper binding energy and be separated from the 5σ component by at least 0.4 eV.[37] This energy order of the CO 1π and 5σ orbitals is consistent with that observed in free gaseous CO; however, in most studies of CO adsorption on transition-metal surfaces, the 5σ photoemission peak lies below the 1π level.

Iterative peak fitting[38] of the angular-dependence data in Figure 2 yields a splitting of 0.7 eV between the CO 5σ and 1π components of peak B. Thus the CO 5σ, 1π, and 4σ bands on CuCl(111) are respectively assigned at 14.5, 15.2, and 18.0 eV below the vacuum level. The energy splitting between 1π and 4σ is approximately the same as that of free CO (~2.8 eV), while the CO 5σ shifts to deeper binding energy by 2.2 eV, 0.9 eV greater than the shift for CO on ZnO (see section C1).

From Figure 2 the intensity of peak C is also dependent on the incidence–detection geometry and is enhanced with increasing detection angle relative to the surface normal. This angular dependence indicates that peak C, which is only present with CO adsorption, originates from a state of π symmetry and, consequently, can be assigned as Cu $3d_\pi$ levels which are downward-shifted as a result of a bonding interaction with the CO $2\pi^*$ level. Further evidence for π back-bonding is obtained from the XPS studies described in section B3.

2. Coverage Dependence and Heat of Adsorption. The PES spectra of the CO/CuCl(111) system are strongly dependent on the ambient CO pressure and sample temperature, indicating reversible CO adsorption. This allows a thermodynamic study of the equilibrium, employing UPS to quantitatively monitor the CO surface coverage. Fixed ambient CO pressures were maintained while UPS spectra were collected at a series of temperatures. Figure 4 presents the CO 4σ peak area vs temperature for two ambient CO pressures (4×10^{-9} and 6×10^{-7} mbar). The heat of adsorption at a given coverage, $\Delta H(\theta)$, can then be determined by using the Clausius–Clapeyron equation

$$[\Delta \ln P/\Delta(1/T)]_\theta = -\Delta H(\theta)/R$$

A linear decrease of $\Delta H(\theta)$ with increasing coverage is found from the data in Figure 4. For a well-formed single-crystal surface this decrease should be due to a repulsive dipole–dipole interaction between CO molecules and can be described by the Temkin isobar expression[39]

$$\Delta H(\theta) = \Delta H_0(1 - \alpha\theta)$$

where α is a constant and ΔH_0 is the heat of adsorption at zero coverage. From CO/CuCl(111) data in Figure 4 the heat of adsorption extrapolated to zero coverage is found to be 23 ± 2 kcal/mol. This ΔH_0 value indicates that the binding between CO and CuCl is weaker than that for CO on most transition metals,[40-42] but stronger than that for CO on ZnO[1] or Cu metal.[40] It is consistent with the value we have observed for Cu(I) sites on the ZnO(0001) and $(10\bar{1}0)$ surfaces.[7] Consequently, the CO/CuCl(111) is a reasonable model for the Cu(I) site on the methanol synthesis catalyst.

3. CO Surface Dipole Moment. Figure 5 presents the HeI spectra of clean and CO-covered CuCl. The onset of the secondary electron tail corresponds to electrons with zero kinetic energy. Therefore the vacuum level is 21.2 eV (the He I photon energy) above this onset. The shift in the electron tail upon adsorption represents a shift in the vacuum level relative to a fixed Fermi level and gives the work function change. For a p-type semiconductor such as CuCl, the surface work function change $\Delta\Phi$ is given by

$$\Delta\Phi = \Delta\Phi_{dipole} - \Delta\Phi_{bb}$$

where $\Delta\Phi_{dipole}$ is the change in the surface dipole moment due to chemisorption and $\Delta\Phi_{bb}$ is the contribution from surface band bending. The change in the band bending can be determined from the valence band peak shift provided the shape of the valence band peak does not change significantly with adsorption. CO chemisorption on CuCl(111) causes a decrease in the downward band bending. In Figure 5 changes due to band bending are corrected by aligning the Cl 3p band of the CO-covered surface with that of the clean surface. The energy shift of the low kinetic energy limit of the secondary electron tail now gives the change in the surface dipole moment. A 0.8 ± 0.2 eV shift of the secondary tail is observed in Figure 5, indicating that there is a 0.8-eV decrease in the surface dipole moment due to CO adsorption on CuCl(111) at 140 K and 1×10^{-7} mbar ambient of CO which corresponds to approximately 0.9 of a monolayer coverage.

(37) We observe a similar angular dependence of the valence band for CO/CuCl(111) using synchrotron radiation which is highly polarized. In agreement with our He II UPS studies, the peak B intensity at larger emission angles is stronger and at approximately 0.4 eV deeper energy, also indicating that the CO 1π level is at least 0.4 eV to deeper binding energy than the CO 5σ orbital.

(38) The iterative fitting procedure varies the position, width, and height of two component peaks with Gaussian/Lorenzian shapes minimizing the difference between the fit and the experimental spectra.

(39) Hayward, D. O.; Trapnell, B. M. W. In *Chemisorption*, 2nd ed.; (1964), Butterworths: Washington, 1964; p 218.

(40) Ishi, S.; Ohno, Y.; Viswanathan, B. *Surf. Sci.* **1985**, *161*, 349.

(41) Toyoshima, I.; Somorjai, G. A. *Catal. Rev. Sci. Eng.* **1979**, *19*, 105.

(42) Nieuwenhuys, B. E. *Surf. Sci.* **1981**, *105*, 505 and references therein.

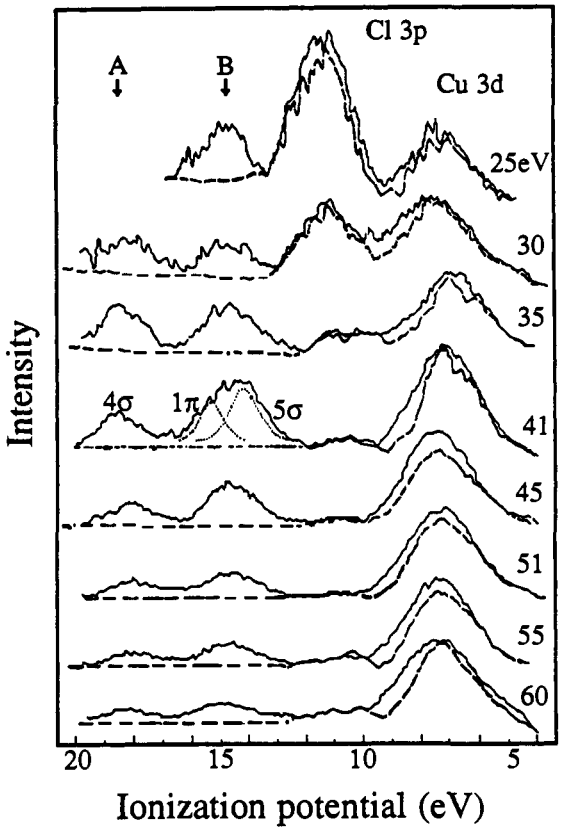

Figure 6. Photon energy dependence of the valence band spectra of CO-saturated CuCl(111) (9000 L CO exposure at 80 K) (solid line) and clean CuCl(111) (broken line) surfaces. In each set of spectra data are normalized and aligned to the Cl 3p band. For the 25-eV spectrum peak A is obscured by overlap with the intensive tail of secondary electrons. Peak B is resolved into two peaks as shown in the 41-eV spectrum, with an energy separation of 2.8 eV for the 1π–4σ (peak A) splitting and 0.7 eV for the 5σ–1π splitting.

From this surface dipole moment change, the CO–Cu(I) molecular dipole moment μ can be determined by using the Helmholtz equation[43]

$$\Delta\Phi_{\text{dipole}} = 4\pi c_s \theta \mu \cos\beta$$

where c_s is the number of surface sites per cm^2, θ is the fractional coverage of the surface (i.e. 0.9 of a monolayer coverage from the He II thermodynamic studies), and β is the angle between the C–O axis and the surface normal (i.e. $\beta = 0$ from the angular dependent He II studies). This gives a value for the apparent dipole moment of $\mu = 0.31$ D negative side down. Assuming that this change in surface dipole moment results mainly from net charge donation from the 5σ orbital on the carbon atom of adsorbed CO to the Cu(I) site, one can estimate the net positive charge on the chemisorbed carbon to be $q = 0.03$ (using $\mu = qL$ where L is the carbon–Cu(I) bond length estimated to be 1.8 Å[44]). This estimate is complicated, however, by additional possible contributions to this change from changes in the intrinsic CO dipole moment and substrate surface dipole moment upon adsorption.[45] A more direct determination of the charge on the carbon upon CO chemisorption is obtained from C 1s XPS studies in section IIIB3.

B. Variable Photon Energy PES Studies of CO/CuCl(111). 1. Valence Band Region. Variable photon energy PES spectra for the CO/CuCl(111) system at 80 K have been recorded from 25 to 150 eV and are presented in Figure 6. The results of variable photon energy PES studies for clean CuCl have been reported previously.[22] Figure 6 shows a significant dependence of the intensity of both peak A (CO 4σ) and peak B (CO 1π, 5σ) on photon energy. The CO 4σ peak intensity is plotted as a function of photon energy in Figure 7a. At lower photon energies the CO 4σ intensity is weak, rising with increasing photon energy until a maximum is reached at 37 eV and then decreasing with further increase in photon energy. This behavior corresponds to a shape resonance which is characteristic of the CO 4σ photoemission band, and thus confirms this assignment of peak A. For gaseous CO, the 4σ shape resonance occurs at a photon energy of 32 eV.[46] On metal surfaces a 4–7 eV shift of the shape resonance to higher photon energy is normally observed.[47-52] The intensity profile for peak B (CO $1\pi + 5\sigma$) vs photon energy is presented in Figure 7b and importantly exhibits two maxima. The first maximum appears at 26 eV, in agreement with the value reported for the shape resonance of the CO 5σ peak on metal surfaces.[47-52] The second maximum appears at a photon energy of 41 eV and is characteristic of a delayed maximum associated with 3d photoemission. The observation of the CO 5σ shape resonance is unambiguous evidence that the CO 5σ photoemission feature contributes to peak B. Additionally, the appearance of the delayed 3d maximum in the peak B intensity–energy profile indicates significant covalent mixing of the Cu 3d and CO 5σ levels.[53] This interaction with the filled 3d levels will also contribute to the 2.2-eV stabilization of the CO 5σ level relative to

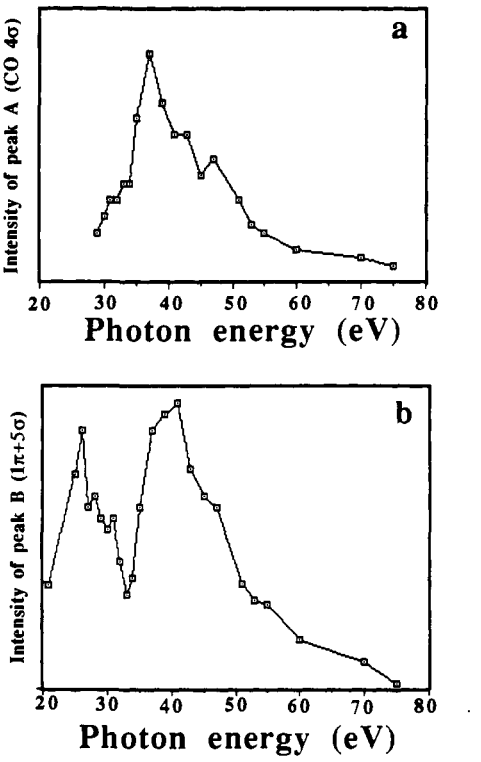

Figure 7. The intensity–energy profiles of CO-derived peaks for CO/CuCl(111) (80 K, 9000 L CO exposure): (a) peak A (CO 4σ), and (b) peak B (CO $1\pi + 5\sigma$).

(43) Thomas, J. M.; Thomas, W. J. In *Introduction to The Principles of Heterogeneous Catalysis*; Academic Press: New York, 1969.
(44) Pasquali, M.; Floriani, C.; Gaetani-Manfredotti, A. *Inorg. Chem.* **1980**, *19*, 1191 and references therein.
(45) Baetzold, R. C. *J. Phys. Chem.* **1983**, *87*, 3858.
(46) Plummer, E. W.; Gustafsson, T.; Gudat, W.; Eastman, D. E. *Phys. Rev. A* **1977**, *15*, 2339.
(47) Plummer, E. W.; Eberhardt, W. *Adv. Chem. Phys.* **1982**, *49*, 533 and references therein.
(48) Greuter, F.; Heskett, D.; Plummer, E. W.; Freund, H. J. *Phys. Rev. B* **1983**, *27*, 7117.
(49) Hofmann, P.; Gossler, J.; Zartner, A.; Glanz, M.; Menzel, D. *Surf. Sci.* **1985**, *161*, 303.
(50) Allyn, C. L.; Gaustafsson, T.; Plummer, E. W. *Solid State Commun.* **1978**, *28*, 85.
(51) Schichl, A.; Menzel, D.; Rosch, N. *Chem. Phys. Lett.* **1984**, *105*, 285.
(52) Umbach, E.; Schichl, A.; Menzel, D. *Solid State Commun.* **1980**, *36*, 93.
(53) Plummer, E. W.; Salaneck, W. R.; Miller, J. S. *Phys. Rev. B* **1978**, *18*, 1673.

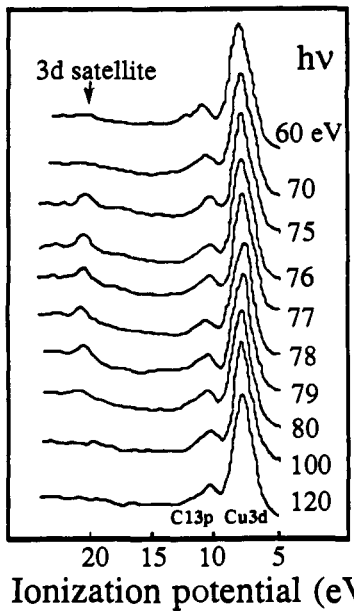

Figure 8. Resonance PES of the CuCl(111) valence band and satellite region. The intensity of the Cu 3d satellite at IP = 20.4 eV is resonance enhanced between 76 and 79 eV photon energy.

the gas phase (vide supra) but will not contribute to the net σ bonding of CO to the Cu(I) surface site, as the interaction between filled levels is weakly antibonding. Net σ bonding requires that the CO 5σ level interacts with the unoccupied Cu 4s (and 4p)[54] levels, which can be experimentally probed as described below.

2. CIS Resonance Studies of the Cu 3p → 4s Transition. Constant initial state experiments were performed on the Cu 3d shake-up satellite peak, which appears at 20.4 eV below the vacuum level, approximately 13 eV to deeper binding energy than the peak maximum of the Cu 3d band (Figure 8). The 3d shake-up satellite intensity is resonance enhanced at photon energies close to the Cu 3p → 4s absorption threshold, while at photon energies away from resonance the satellite intensity is very weak. For CuCl, the Cu 3p photoemission peak lies at 79.7 eV below the vacuum level. Maximum resonance enhancement of the 3d satellite occurs at about 77 eV. The mechanism of this resonance enhancement is given in Scheme I. At the Cu 3p

Scheme I

Cu 3p threshold excitation: $3p^63d^{10}4s^0 + h\nu \rightarrow 3p^53d^{10}4s^1$

SCK Auger decay: $3p^53d^{10}4s^1 \rightarrow 3p^63d^84s^1$

Cu 3d ionization plus shake-up: $3p^63d^{10}4s^0 \rightarrow 3p^63d^84s^1$

absorption edge, a 3p core-level electron is excited into the Cu 4s bound state. This excited state then decays via a super Coster Kronig (SCK)[55] Auger decay process involving two electrons. The final state produced is the same as that achieved through a 3d ionization plus 3d-to-4s shake-up process which corresponds to the satellite peak in Figure 8. Constructive interference of these two pathways results in the resonance enhancement of the 3d satellite intensity at the Cu 3p absorption edge. Since the resonance observed for CuCl arises from the 3p → 4s transition, the approximate energy (ignoring relaxation effects resulting from the transition to a bound state) of the 4s level can be determined, as can the effect on this level of binding CO to the surface. Note that the kinetic energy of ejected electrons in these experiments

(54) The metal 4p level of σ symmetry will hybridize with the 4s level. We observed the 4s energy directly in our CIS studies in section III B2. For Cu(I) and Zn(II) the 4p level is located at about the same energy position above the Fermi level, based on atomic spectral data (Moore, C. E. In *Atomic Energy Levels*, 1952). Therefore we treat the 4s as representative of the 4s and 4p hybridized orbitals participating in σ bonding CO to the metal ion surface site.

(55) Ghosh, P. In *Introduction to Photoemission Spectroscopy*; Wiley: New York, 1983.

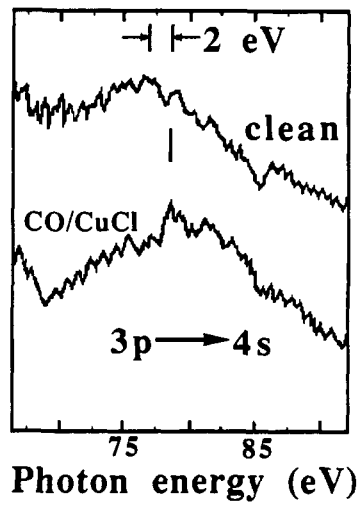

Figure 9. Constant initial state (CIS) intensity profile of the satellite in Figure 8 at the Cu 3p → 4s absorption edge for the CuCl(111) surface before and after CO adsorption. Upon CO adsorption, the intensity maximum corresponding to the Cu 3p → 4s transition shifts to higher photon energy.

is ~50 eV; therefore this experiment probes the 4s level with high surface sensitivity.

The resonance intensity–photon energy profiles for the 3d shake-up satellite of CuCl(111) before and after CO adsorption at 80 K are shown in Figure 9. Upon CO adsorption, the 3p → 4s transition shifts by 2.0 ± 0.3 eV to higher photon energy. Since the energy of the Cu 3p core level does not change due to CO adsorption, the increased energy splitting of the 3p → 4s transition must result from a shift of the 4s level to higher energy. This provides direct evidence that the unoccupied Cu 4s is involved in a bonding interaction with the CO 5σ orbital.

For a coordinatively unsaturated tetrahedral Cu(I) site with C_{3v} symmetry, the Cu $3d_{z^2}$, 4s, and $4p_z$[54] orbitals have the same symmetry as the CO 5σ orbital and therefore all participate in σ bonding with CO. This is found experimentally by the appearance of a delayed 3d maximum in the CO 5σ intensity–energy profile (Figure 7b), the upward shift of the resonance maximum of the 3p → 4s transition, and the downward energy shift of the CO 5σ level. Both the Cu 3d and 4s orbitals can contribute to the CO 5σ stabilization, since both lie at higher energy than the CO 5σ level. However, since the closed-shell interaction of the Cu 3d orbitals results in a net repulsive contribution to the CO bonding, the CO 5σ shift is not a reliable probe of chemical bonding. Alternatively, the observed Cu 4s destabilization is predominantly a result of an antibonding interaction with the CO 5σ state. As the 4s level is unoccupied for groups IB and IIB metal ions, one can estimate the net σ bonding of CO/CuCl from its destablization and compare this with the results for CO on ZnO (see section IIIC2).

3. C 1s and O 1s Core Level PES Studies of the Effective Atomic Charge. Figure 10 presents XPS data on the O 1s (CO 1σ) and C 1s (CO 2σ) core levels for the CO-saturated CuCl(111) surface. Both the C 1s and O 1s photoemission spectra exhibit strong satellite structure. In the C 1s spectrum, the main peak is at 291.8 eV below the vacuum level and is followed by a satellite that is 4.8 eV to deeper binding energy with an intensity of 50% relative to that of the main peak. In the O 1s PES spectrum, the satellite is separated from the main peak (at 538.9 eV below the vacuum level) by 5.6 eV with an intensity relative to the main peak of 64%.

The satellite structure of CO core levels has been reported for many transition-metal surfaces and has been attributed to the presence of two final states: unscreened and screened.[56-60] For

(56) Brundle, C. R.; Bagus, P. S.; Menzel, D.; Hermann, K. *Phys. Rev. B* **1981**, *24*, 7041.

(57) Bagus, P. S.; Seel, M. *Phys. Rev. B* **1981**, *23*, 2065.

(58) Plummer, E. W.; Chen, C. T.; Ford, W. K.; Eberhardt, W.; Messmer, R. P.; Freund, H. J. *Surf. Sci.* **1985**, *158*, 58.

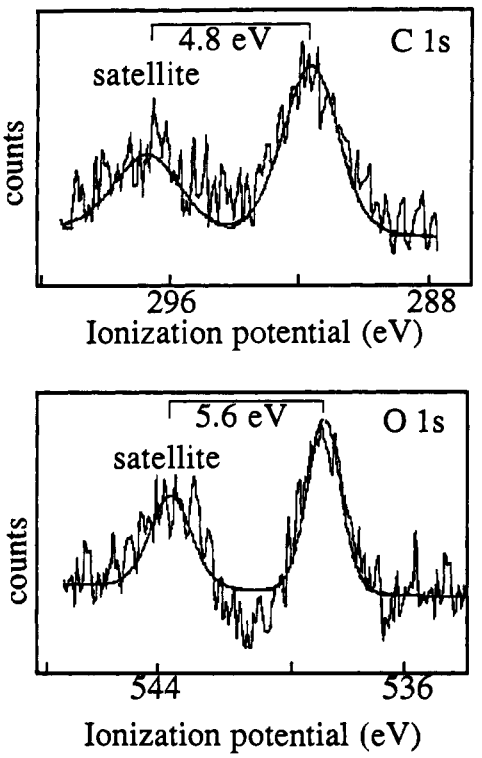

Figure 10. XPS C 1s and O 1s spectra for CO/CuCl(111) at 140 K and 1×10^{-7} mbar ambient CO. The spectra were taken with large analyzer pass energy (50 eV, which corresponds to a 1.8 eV instrument resolution) and signal averaged over 40 scans in order to increase the signal to noise. The C 1s spectrum shows a strong satellite at 4.8 eV to deeper binding energy with an intensity ratio of 64%.

the latter, the core hole created by photoemission is screened through charge transfer from the metal d band into the unoccupied CO $2\pi^*$ level. The $2\pi^*$ level of the chemisorbed CO molecule lies energetically between the Fermi level and the vacuum level before the core exitation.[61-65] It is usually stabilized to a lower energy than the metal d band, as a result of relaxation due to the core excitation. Compared to the unscreened final state, the photoelectrons from the screened state have a higher kinetic energy and correspond to the peak at lower binding energy. This is the main peak in the spectrum and is often referred to as a shake-down peak.

Since the covalent bonding interaction between the Cu d_π and the CO $2\pi^*$ excited state provides the intensity mechanism for the screened core-hole final state, the existence of the CO core level satellite structure for the CuCl(111) surface is strong evidence for the presence of significant π back-bonding. Further, the intensity distribution between the main and satellite peaks of CO core levels is closely related to the extent of $2\pi^*$ back-bonding in the ground state (see Discussion, section IV), the weaker the bonding, the lower the probability for charge transfer screening, and therefore, the more intense the unscreened satellite peak at higher binding energy.[56-60] The CO/Ni(100) system usually serves as an example of strong d-π bonding, with a C 1s satellite peak intensity of 35% (I_{sat}/I_{main}).[56] Alternatively, the satellite peak of the CO core level is found to be even more intense than the main peak for CO/Ag(110),[66] which is an example of poor d-π mixing. Therefore, the d-π back-bonding in the CO/CuCl(111) system appears to be of intermediate strength, based on the C 1s satellite structure (I_{sat}/I_{main} = 50%).

According to the sudden approximation,[22,67] the binding energy of the C 1s peak in the initial state is given by the photoemission intensity weighted average energy including both main and satellite lines. For the CO/CuCl(111) system, this is calculated to be 293.4 ± 0.3 eV below the vacuum level. Compared with gaseous CO (BE for C 1s = 295.9 eV),[68] the C 1s line of CO/CuCl appears at 2.5 eV lower energy. The total binding energy shift for a nonbonding level on chemisorption, ΔBE_{PES}, results from an extramolecular relaxation polarization shift, ΔR (a final state effect, in which the core hole on the adsorbate molecule created by photoemission is partly screened through polarization of electrons from the substrate, resulting in a peak shift to lower binding energy), and from effects of the change in chemical environment, ΔE (an initial state effect caused by redistribution of valence electron density between an adsorbate molecule and the substrate due to bonding, shifting the peak to deeper binding energy as the net positive charge on the atom increases):

$$\Delta BE_{PES} = \Delta E - \Delta R \quad (1)$$

The effective atomic charges of the adsorbed CO are closely related to ΔE, rather than to the total energy shift ΔBE_{PES}.

The core relaxation, ΔR_c, can be obtained from the energy shift of a corresponding Auger line. The energy shift in an Auger line is usually larger than that for related photoemission lines because the Auger transition involves larger extramolecular relaxation effects.[69-72] On the basis of a classical electrostatic model, the polarization energy, R, of an ion in a dielectric solid is quadratically dependent on the total hole charge e,

$$R = \tfrac{1}{2}(e^2/d)[1 - (1/k_o)] \quad (2)$$

where d is the effective hole radius (proportional to the distance of the hole to its nearest neighboring atom) and k_o is the dielectric constant at optical frequencies.[73,74] As an Auger line involves two holes in its final state, the extramolecular relaxation for an Auger process should be approximately 4 times larger than that for a photoemission process. From the above equation it is also noted that core levels normally show larger relaxation shifts, ΔR_c, than valence levels, ΔR_v,[58,75,76] since the relaxation energy is inversely proportional to d ($\Delta R_c/\Delta R_v = d_v/d_c$) and the more delocalized valence levels should have larger effective hole radii, d_v. From above, the total peak energy shift relative to the gas-phase value for an Auger line involving valence levels (in particular the carbon KVV peak of CO/CuCl(111)), ΔKE_{Auger}, can be approximated by

$$\Delta KE_{Auger} \simeq -\Delta BE_v + 4\Delta R_v - \Delta R_c \quad (3)$$

where ΔBE_v denotes the change in binding energy for a nonbonding CO valence level. From known Cu(I) carbonyl structures

(59) Norton, P. R.; Tapping, R. L.; Goodale, J. W. *Surf. Sci.* **1978**, *72*, 33.
(60) Umbach, E. *Surf. Sci.* **1982**, *117*, 482.
(61) Netzer, F. P.; Matthew, J. A. D.; Bertel, E. In *Spectroscopies of Surfaces*; Clark, R. J. H., Hester, R. H., Eds.; John Wiley and Son Ltd.: New York, 1988.
(62) Dose, V. *Surf. Sci. Rep.* **1985**, *5*, 337 and references therein.
(63) Rogozik, J.; Dose, V. *Surf. Sci.* **1986**, *176*, L847.
(64) Avouris, Ph.; Demuth, J. E. *Surf. Sci.* **1985**, *158*, 21.
(65) Ferrer, S.; Frank, K. H.; Rhihl, B. *Surf. Sci.* **1985**, *162*, 264.
(66) Krause, S.; Mariana, C.; Prince, K. C.; Horn, K. *Surf. Sci.* **1984**, *138*, 305.
(67) Freund, H. J.; Plummer, E. W.; Salaneck, W. R.; Bigelow, R. W. *J. Chem. Phys.* **1981**, *75*, 4275.
(68) Siegbahn, K.; Nordling, C.; Johansson, G.; Hedman, J.; Heden, P. F.; Hamrin, K.; Gelius, U.; Bergmark, T.; Werme, L. O.; Manne, R.; Baer, Y. In *ESCA Applied to Free Molecules*; North-Holland Publishing Company: Amsterdam, 1969.
(69) Martin, R. L.; Shirley, D. A. In *Electron Spectroscopy: Theory Techniques and Applications*; Brundle, C. R., Baker, a. D., Eds.; Academic Press: New York, 1977; Vol. 1, p 75.
(70) Kowalczyk, S. P.; Ley, L.; Mcfeely, F. R.; Pollak, R. A.; Shirley, D. A. *Phys. Rev. B* **1974**, *9*, 381.
(71) Fuggle, J. C. In *Electron Spectroscopy: Theory, Techniques and Applications*; Brundle, C. R., Baker, A. D., Eds.; Academic Press: New York, 1981; Vol. 4, p 85.
(72) Thomas, T. D. *J. Electron Spectrosc. Related Phenom.* **1980**, *20*, 117.
(73) Wagner, C. D.; Biloen, P. *Surf. Sci.* **1973**, *35*, 82.
(74) Mott, N. F.; Gurney, R. W. *Electronic Processes in Ionic Crystals*; Clarendon: Oxford, 1948.
(75) Miller, J. N.; Ling, D. T.; Stefan, P. M.; Weissman, D. L.; Shek, M. L.; Lindau, I.; Spicer, W. E. *Phys. Rev. B* **1981**, *24*, 1917.
(76) Norton, P. R.; Tapping, R. L. *Chem. Phys. Lett.* **1976**, *38*, 207.

(the bond lengths of Cu–C and C–O are 1.8 and 1.1 Å, respectively)[44] we obtain from eq 2 that $\Delta R_c \sim 1.7\Delta R_v$. Therefore, ΔR_c can be estimated from the experimental energy shift in the Auger line (ΔKE_{Auger}) and a nonbonding photoemission valence peak (ΔBE_v).

Experimentally, the carbon KVV Auger lines of CO/CuCl(111) were observed by using synchrotron radiation. ΔKE_{Auger} is determined to be a 5.6 ± 0.5 eV shift to higher kinetic energy relative to gas-phase CO.[58,68] The change in the CO nonbonding photoemission valence level binding energies (i.e. the CO 4σ and 1π levels in Figure 1) is −1.7 eV as compared with CO gas. ΔR_c obtained from the above equation is −2.9 eV. Hence, of the 2.5-eV shift in energy to lower binding energy found for the C 1s PES initial state of CO/CuCl(111), 2.9 eV is due to extramolecular polarization relaxation shift; thus a 0.4-eV shift to deeper binding energy is caused by a change in the chemical environment of the carbon due to chemisorption, indicating that the carbon atom carries a net positive charge.

It is possible to estimate the effective atomic charge, Q, on the carbon atom of CO according to the charge potential model:[68,77]

$$\Delta E_{PES} = kQ + V + L$$

where ΔE_{PES} is the shift in the core-level ionization potential of an atom with respect to that of a standard compound (CH_4 at 290.7 eV)[68] which serves as the origin of the energy scale. V is the coulomb potential energy at the vacated site of the atom in the presence of the other atoms of the compound ($V = \sum(Q'/r)$, in which Q' is the charge on an atom estimated from the half-ionized core model,[77] r is its distance from the vacancy, and the sum is over all atoms).[78] k and L are Jolly's empirical parameters determined from a least-squares fit for a large series of chemical shifts of an element (k = 24.95 and L = 3.44). The effective atomic charge on the carbon atom of CO/CuCl(111) calculated by using ΔE_{PES} = +5.6 eV shift to deeper binding energy (relative to CH_4 for the relaxation corrected chemisorbed CO) is Q = +0.26 unit charge. The effective atomic charge on the carbon atom of gas-phase CO calculated by using the same procedure is +0.16. The net increase in the positive charge on the carbon ΔQ = 0.10 corresponds to the electron density transferred from adsorbed CO to the CuCl surface and is consistent with the results obtained from work function measurements in section IIIA3 in that both give a small net positive charge on the carbon of bound CO. The atomic charge obtained by using the charge potential model has been shown to correlate well to the values obtained from Pauling electronegativities and ab initio calculations.[68]

4. NEXAFS Study of the Chemisorbed C–O Bond Length. The NEXAFS spectra for CO/CuCl(111) at 130 K shown in Figure 11 were collected with synchrotron radiation at two different incidence–detection geometries: a relatively large angle of photon incidence relative to the surface normal (Figure 11a, A vector of light is at 43° off the surface normal), and a small angle of incidence with respect to the surface normal (Figure 11b, A vector of light at 71° off the surface normal). A broad resonance feature which is centered at ~308.5 ± 0.5 eV appears in both spectra but is more intense in spectrum a. Dipole selection rules require that the intensity of a σ shape resonance be stronger when the orientation of the A vector of light is close to the molecular axis.[79] Since the axis of the bound CO molecule is normal to the CuCl(111) surface based on the angular dependent UPS data in Figure 2, the broad feature in Figure 11 can be attributed to a σ shape resonance.

The energy of the shape resonance is governed by the intramolecular C–O bond length.[80,81] Stöhr et al. have developed a

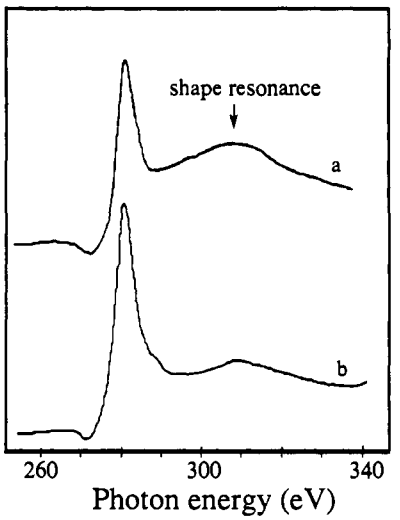

Figure 11. Carbon K edge NEXAFS spectra of CO/CuCl(111) (9000 L exposure at 130 K) taken at (a) large incidence angle (47°) off the surface normal and (b) small incidence angle (19°) off the surface normal.

semiempirical equation based on multiple scattering theory to relate the resonance energy and the bond length,[79,81]

$$(\delta - V_0)r^2 = C_0$$

where δ is the energy difference between the shape resonance and the C 1s core level, r is the intramolecular bond length, and C_0 and V_0 are constants, equal to 35.7 ± 2.3 eV·Å^2 and −9.2 ± 1.6 eV, respectively. This equation allows bond length determinations to within 0.05 Å.[79] On the basis of the energy positions of the shape resonance in Figure 11 and of the satellite-corrected C 1s XPS peak in Figure 10, δ = 19.8 ± 0.5 eV and the C–O bond length for carbon monoxide chemisorbed on the CuCl(111) surface is calculated to be 1.11 ± 0.05 Å. If the bond length of the chemisorbed CO were at its gas-phase value of 1.13 Å, the above formalism would predict a value of δ of 18.9 eV.[82] The larger experimental value of δ of 19.8 eV requires that the CO bond length has measurably decreased from its gas-phase value upon CO chemisorption to CuCl(111).

C. Variable Photon Energy PES Studies of CO/ZnO(10$\bar{1}$0). 1. Valence Band Region. The electronic structure of CO/ZnO surfaces has been investigated in detail using He I and He II UPS.[1] Here we extend these studies on CO/ZnO(10$\bar{1}$0) to include variable photon energy PES experiments to parallel those on CO/CuCl(111) in section **B**. In the earlier UPS studies of CO/ZnO, difficulties arose in examining the CO 5σ photoemission peak because of its overlap with the Zn 3d band, and only a lower limit of >0.5 eV relative to the gas phase could be estimated for its energy stabilization due to bonding to the Zn(II) surface site. However, at lower photon energies the photoemission cross section for the CO 5σ peak is relatively large in comparison to the d band, which allows a clear determination of the binding energy of the CO 5σ level. Figure 12 presents valence band photoemission spectra for the clean and CO-covered ZnO(10$\bar{1}$0) surfaces taken at a series of photon energies. The valence band spectra of clean ZnO consist of two major peaks, the Zn 3d band centered at 10.7 eV and the O 2p band between 4 and 8 eV relative to the Fermi level.[83] Upon CO adsorption new features appear with a well-separated CO 4σ peak located at 14.7 eV below the Fermi level. Comparison of the valence band spectra at a given photon energy for the clean and CO-covered surfaces indicates that significant changes in the Zn 3d region also occur with variation in photon

(77) Jolly, W. L. *Faraday Discuss. Chem. Soc.* **1972**, *54*, 13.

(78) Using $Q_O' = -1.2$, $Q_{Cl}' = -0.8$, $Q_{Cu}' = 0.6$, $r_{Cu-C} = 1.8$ Å, $r_{O-C} = 1.1$ Å, and $r_{Cl-C} = 3.3$ Å we obtain $V = \sum Q'/r = -4.6$ for the carbon site in the $[O–C–CuCl_3]^{2-}$ cluster. Note that all Q's estimated from the half-ionized core model should be multiplied by 0.2 when used to obtain V.[77]

(79) Stöhr, J. In *The Structure of Surfaces*; ed. by Van Hove, M. A., Tong, S. Y., Eds.; Springer-Verlag: Berlin, 1985; p 140.

(80) Stöhr, J.; Jaeger, R. *Phys. Rev. B* **1982**, *26*, 4111.

(81) Stöhr, J.; Gland, J. L.; Eberhardt, W.; Outka, D.; Madix, R. J.; Sette, F.; Koestner, R. J.; Dobler, U. *Phys. Rev. Lett.* **1983**, *51*, 2414.

(82) This lower value of δ is consistent with the value obtained for CO on Ni(100) of 17.2 eV where the CO bond length is increased from its gas-phase value.

(83) The energy levels of ZnO are all referred to the Fermi level, in agreement with our previous publications on ZnO, since charging effects are not observed for ZnO even at low temperatures.

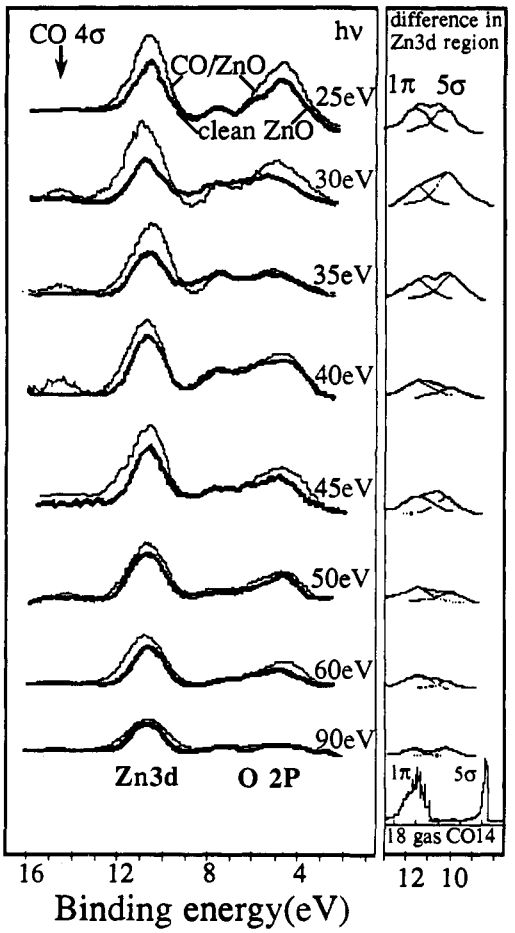

Figure 12. Photon energy dependence of the valence band photoemission spectra for the CO-covered (9000 L CO exposure, 80 K) and clean (bold lines) ZnO ($10\bar{1}0$) surfaces. The spectra of CO-covered surfaces are normalized to the incident photon flux. The spectra of the clean surfaces are aligned and normalized to the least-perturbed part of the oxide band (at 7–8 eV). Presented in the right panel are the CO-covered minus clean difference spectra in the Zn 3d band energy region. In the bottom right panel are the He II 1π and 5σ photoemission peaks of CO gas[32] with the 1π peak aligned to that of CO/ZnO, which corresponds to a −0.6 eV shift relative to the gas phase. Also included in the right panel are the results of the $1\pi/5\sigma$ fit as described in the text.

energy.[84] The CO-covered minus clean difference spectrum in the Zn 3d region is included to the right of each set of spectra. The difference intensity in this energy region should originate from the CO 1π and 5σ photoemission peaks. The CO 1π contribution is not involved in bonding and should appear at its gas-phase value at ~2.8 eV lower binding energy relative to the CO 4σ peak, which puts the 1π at ~11.9 eV below the Fermi level, on the high bonding energy side of the Zn 3d band. Therefore, the intensity increase at the low binding energy side of the Zn 3d band must derive from CO 5σ photoemission. The difference spectra were fit with two Gaussian/Lorenzian peaks by a procedure that fixed the 1π position (at its gas-phase separation from the 4σ) and varied the peak widths, heights, and the energy position of the 5σ level. These fits are included with the difference spectra to the right in Figure 12. With respect to the Fermi level, the CO 5σ level is found at 10.3 ± 0.3 eV, which corresponds to a 1.3-eV shift to deeper binding energy from its value for free CO (included at the bottom right of Figure 12), significantly smaller than the 2.2-eV 5σ shift observed for CO/CuCl(111) in Figure 6.

From Figure 12, the intensity of the CO 4σ peak varies with photon energy, reaching a maximum at 40 eV and then decreasing at higher photon energies. The intensity–energy profile for CO

(84) Changes in the oxide valence band region are also evident, which result from changes in substrate photoemission due to CO binding.

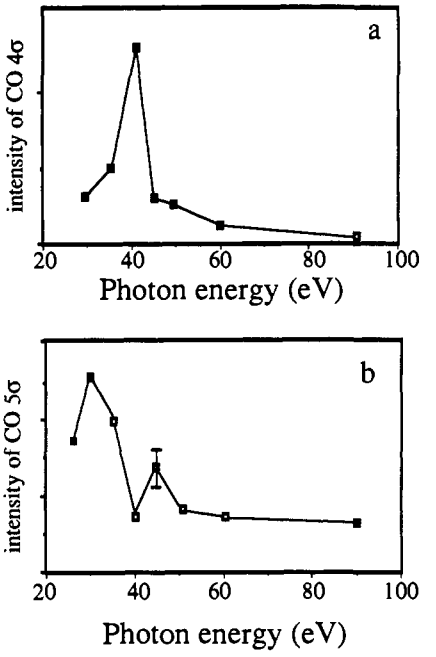

Figure 13. Intensity–energy profiles for CO/ZnO($10\bar{1}0$) (9000 L CO exposure, 80 K): (a) CO 4σ level, (b) fit CO 5σ peak from Figure 12, right panel.

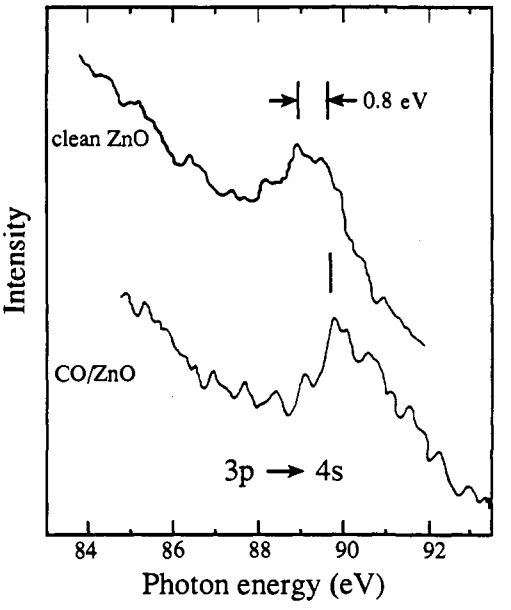

Figure 14. Constant initial state intensity profile of the valence band shake-up satellite (BE = 31.7 eV) through the Zn 3p → 4s absorption edge for the ZnO($10\bar{1}0$) surface before and after CO adsorption (9000 L, 80 K). Upon CO adsorption, the intensity maximum corresponding to the Zn 3p → 4s transition shifts by 0.8 eV to higher photon energy.

4σ is shown in Figure 13a where the intensity maximum at 40 eV photon energy can be assigned as a σ shape resonance, as observed for CO on CuCl(111) in Figure 7a. Figure 13b presents the intensity of the fit 5σ peak of CO in Figure 12 right as a function of photon energy. This profile exhibits maxima at 30 and 45 eV, which are assigned in parallel to the $5\sigma + 1\pi$ cross section for CO on CuCl(111) in Figure 7b as the CO 5σ shape resonance and 3d delayed maximum, respectively. However Figure 13b is different from Figure 7b in that the 3d delayed maximum for CO/ZnO is small compared to that for CO on CuCl, which indicates that there is very little mixing of the metal 3d orbitals with the CO 5σ level for CO/ZnO.

2. CIS Resonance Studies of the Zn 3p → 4s Transition. The photoelectron spectrum of the valence band region of clean ZnO($10\bar{1}0$) exhibits a 3d shake-up satellite at 31.7 eV (relative

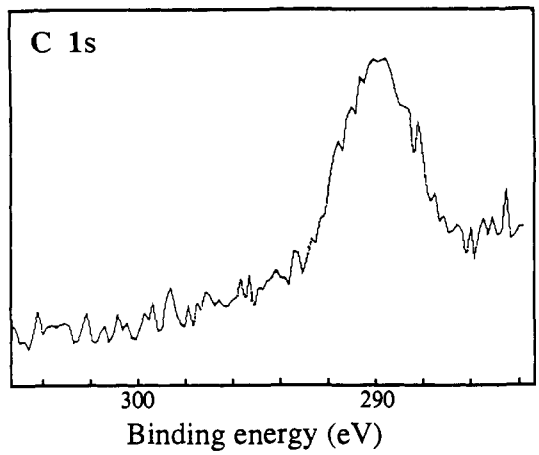

Figure 15. C 1s photoemission spectrum for CO/ZnO(10$\bar{1}$0) (5×10^{-6} Torr ambient CO, 80 K). The spectrum was taken with use of 400 eV synchrotron radiation and signal averaged for 10 scans to increase the signal to noise.

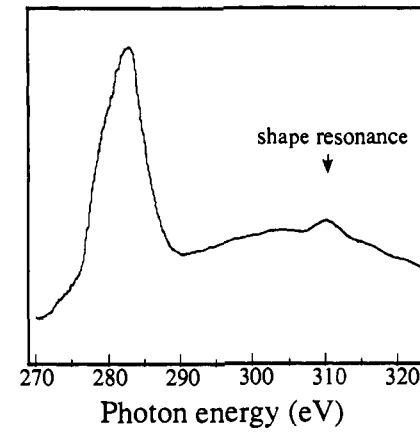

Figure 16. Carbon K edge NEXAFS spectrum of CO/ZnO(10$\bar{1}$0) (80 K, 9000 L CO exposure). The peak centered around 310 eV is assigned as the shape resonance. The feature between 300 and 305 eV is due to the O 2s which is located at ~27 eV below the Fermi level.

to the Fermi level), which becomes resonance enhanced at the Zn M edge at photon energies around 89 eV.[23] The CIS intensity profiles for the Zn 3d shake-up satellite of clean and CO-covered ZnO(10$\bar{1}$0) are shown in Figure 14. A 0.8 ± 0.2 eV shift to higher photon energy of the satellite CIS intensity maximum is observed upon CO adsorption. As with CuCl, Scheme I in section IIIB also holds for the ZnO CIS data, and the shake-up process is described as a $3d^{10} \rightarrow 3d^8 4s^1$ transition, which must be resonance enhanced by absorption at the Zn 3p → 4s edge. Since from XPS data the Zn 3p peak is at 88.6 eV below the Fermi level and does not shift upon CO adsorption, the 0.8-eV shift in the satellite CIS intensity maximum is due to destabilization of the Zn 4s level upon CO binding, indicating the involvement of the Zn 4s orbital in bonding. This is significantly smaller than the 2.0-eV shift observed for CO binding to Cu(I) on CuCl(111) in Figure 9, indicating that the Zn(II)4s–CO5σ interaction is much weaker. This parallels the lower Zn3d–CO5σ mixing based on the cross section data in Figure 13.

3. C 1s Core Level PES Studies of the Effective Atomic Charge. Carbon KVV Auger and C 1s core level PES data for CO/ZnO(10$\bar{1}$0) were measured by using synchrotron radiation. The C 1s core level in Figure 15 is centered at 290.1 ± 0.5 eV relative to the Fermi level (294.5 eV relative to the vacuum level), a shift of 1.4 eV to lower ionization energy from the gas-phase CO value. The spectrum in Figure 15 shows one peak with no evidence of satellite structure, indicating that there is no measurable interaction between the CO $2\pi^*$ and Zn 3d orbitals. The carbon Auger KVV lines for CO/ZnO(10$\bar{1}$0) were observed at 3.6 ± 0.5 eV higher kinetic energy than for free CO. There is a 0.6-eV shift to lower binding energy (relative to gas-phase CO) of the valence 4σ and 1π peaks (see section C1). Following the same procedure described for CO/CuCl in section **B3**, it is found that the extramolecular relaxation polarization shift is 1.2 eV for valence levels and 2.0 eV for the core level. Hence the chemical environment change upon CO adsorption on ZnO(10$\bar{1}$0) results in a 0.6-eV shift to deeper binding energy of the C 1s peak relative to the gas CO. This chemical shift gives an effective atomic charge on the carbon atom of CO/ZnO(10$\bar{1}$0) of $Q = +0.3$.[85] Relative to the gas-phase CO value, the atomic charge on the carbon atom is increased by $\Delta Q = 0.14$, which is larger than that of CO/CuCl(111) ($\Delta Q = 0.10$). This corresponds to a larger charge transfer to the surface relative to the CO/Cu(I) system and is required by the larger chemical shift ($\Delta E = 0.6$ for Zn(II) vs 0.4 eV for Cu(I)). This is also supported by the observation[1] of a larger change in the surface dipole moment ($\Delta\Phi = -1.2$ for Zn(II) vs −0.8 eV for Cu(I)), which gives a larger apparent dipole ($\mu = 0.61$ for Zn(II) vs 0.31 D for Cu(I)). Thus both XPS and work function studies show that more charge is transferred from the CO carbon to Zn(II) than Cu(I), and therefore the carbon atom bound to the Zn(II) site carries more positive charge. This provides significant insight into the role of the Zn(II) and Cu(I) sites in catalytic methanol synthesis and will be discussed in section IVB.

Table I. Comparison of Electronic and Physical Properties of CO Binding to Zn(II), Cu(I), and Ni(0) Sites

property	ZnO(10$\bar{1}$0)	CuCl(111)	Ni(100)[a]
ΔE_{M4s} (eV)	0.8	2.0	*b*
$\Delta E_{CO5\sigma}$ (eV)	1.3	2.2	3.1
ΔE_{M3d} (eV)	*c*	0.8	2.1
$(\Delta E_{sat})_{C1s}$ (eV)	*d*	4.8	5.2
$(I_{sat}/I_{main})_{C1s}$ (%)	<10[d]	50	35
ΔQ (unit charge)	+0.14	+0.10	−0.05[e]
ΔH_0 (kcal/mol)	12	23	28
$\Delta\phi$ (eV)	−1.2	−0.8	+1.0
ΔL_{C-O} (Å)	−0.03	−0.02	+0.03
$\Delta\nu_{C-O}$ (cm^{-1})	+59	*f*	−74

[a] References 40, 42, 50, 56, 58, 81, 86, 87. [b] No experimental data reported. The 4s level is located right below the Fermi level for clean Ni surfaces (with the electronic configuration $3d^9 4s^1$); it should be located above the Fermi level for CO/Ni surfaces ($3d^{10} 4s^0$). [c] Not determined experimentally due to overlap with CO 1π and 5σ. [d] The C 1s satellite is not evident for CO/ZnO. An upper limit to the satellite intensity is estimated from the experimental signal to noise. [e] Calculated from data given in the references listed in footnote *a*. [f] No intramolecular vibrational data could be obtained with use of HREELS for CO chemisorbed on single-crystal CuCl surfaces due to charging (Paul J.; Koel B.; Lin, J.; and Solomon, E. Unpublished results).

4. NEXAFS Study of the C–O Bond Length. Auger yield NEXAFS studies were also performed on CO/ZnO(10$\bar{1}$0) and the results are shown in Figure 16. The intensity maximum at 310 ± 0.5 eV photon energy is assigned to the CO shape resonance in parallel to the NEXAFS data for CO on CuCl(111) in Figure 11. By using the C 1s XPS peak energy in Figure 15, δ is found to be 19.9 eV, considerably larger than the δ value of 18.9 eV corresponding to the gas-phase CO bond length of 1.13 Å (see section IIIB4). Thus as observed for CO on CuCl, the CO bond length is found to contract upon chemisorption to ZnO. A shorter C–O bond relative to the gas-phase value is in agreement with our previous findings[1,6] of an increase in the C–O stretching frequency and intraligand vibrational force constant relative to gas-phase CO and a decrease in the surface dipole moment upon CO chemisorption. It is also consistent with the lack of a C 1s shake-up satellite, indicating that σ bonding plays a dominant role in the binding of CO to Zn(II), removing electron density from

(85) Using $Q_O' = -0.9$, $Q_{O^{2-}}' = -1.9$, $Q_{Zn}' = 1.5$, $r_{Zn-C} = 2.0$ Å, $r_{O-C} = 1.1$ Å, $r_{O^{2-}-C} = 3.5$ Å, and a factor of 0.2 (see ref 77) we obtain $V = \sum Q'/r = -5.42$ for the carbon site in the $[O-C-ZnO_3]^{4-}$ cluster.

(86) Smith, R. J.; Anderson, J.; Lapeyre, G. J. *Phys. Rev. B* **1980**, *15*, 632.

(87) Andersson, S. *Solid State Commun.* **1977**, *21*, 75.

the antibonding 5σ orbital and strengthening the C–O bond.

IV. Discussion

A. Nature of CO Bonding to d^{10} Ions: Cu(I) vs Zn(II). The electronic and physical properties of CO bonding to Zn(II) and Cu(I) coordinatively unsaturated C_{3v} surface sites are summarized in Table I. CO adsorption on ZnO surfaces has been investigated in detail with UPS, Angle-Resolved UPS, variable photon energy PES, and HREELS.[1-7] From our earlier studies it is known that σ donation dominates the bonding of CO to Zn(II), while π back-donation from the metal ion is negligible. This is based on a decrease in the surface dipole moment ($\Delta\phi$) and an increase in the C–O stretching frequency relative to the gas-phase value ($\Delta\nu_{C-O}$), as well as the decrease in C–O bond length (ΔL_{C-O}) determined from the NEXAFS data in section IIIC4. Parallel investigations on the CO/CuCl(111) system show that, in addition to σ bonding, there is evidence for significant π back-bonding. This includes the CO-induced bonding shift of the π-polarized Cu 3d photoemission band to deeper binding energy (ΔE_{M3d}) and the presence of significant satellite intensity ($(I_{sat}/I_{main})_{C1s}$) at higher energy from the main peak (ΔE_{sat}) in the C 1s core level photoemission spectrum for CO/CuCl(111) but not CO/ZnO-($10\bar{1}0$). Sections IIIB and IIIC present and compare the experimental results obtained for CO/CuCl(111) and CO/ZnO-($10\bar{1}0$) with use of synchrotron radiation. These studies have enabled us to quantify the relative contribution of σ and π bonding. The σ-bonding interactions are observed in the stabilization of the CO 5σ orbital ($\Delta E_{CO5\sigma}$) by 2.2 and 1.3 eV on Cu(I) and Zn(II), respectively. However, the involvement of the Cu 3d orbitals in the CO 5σ stabilization is required by the presence of a 3d delayed maximum in the CO 5σ cross section energy profile in Figure 7. Although 3d mixing contributes to the CO 5σ energy stabilization, it makes no contribution to the overall bonding since both Cu(I) and Zn(II) are closed-shell d^{10} ions. Consequently CIS studies on the destabilization of the unoccupied 4s level (ΔE_{M4s}) are important for the quantitative comparison of the net σ bonding for CO on Cu(I) and Zn(II).[54] The σ-bonding interaction for the CO/CuCl system is found to be significantly stronger based on a 2.0-eV shift of the 4s level, vs a 0.8-eV shift for the CO/ZnO($10\bar{1}0$) system. The stronger σ donation plus the presence of π back-bonding, both of which contribute to the net bonding to the Cu(I) surface site, result in the higher heat of adsorption for CO on Cu(I) (ΔH_0). Finally, from Table I it is clear that even for CO binding to Cu(I) σ bonding dominates over π bonding in that the CO bond length is reduced, the surface dipole moment is reduced, and net negative charge is transferred to the surface which is associated with the increased positive charge on the carbon of CO (ΔQ) from XPS data. This is further consistent with the lower energy stabilization of Cu 3d (ΔE_{M3d}) due to π bonding as compared to the destabilization of the Cu 4s level (ΔE_{M4s}) due to the σ-bonding interaction.

The energy changes of the substrate and CO orbitals on binding (ΔE_i's in Table I) can be used to obtain insight into the electronic structure origins of the difference in bonding interactions between these two d^{10} systems. The secular determinant given below gives the interaction energies for σ bonding between the CO 5σ and the metal 3d and 4s orbitals:

$$\begin{vmatrix} E_{4s}-E & H_{s,d} & H_{s,\sigma} & H_{s,s'} \\ H_{d,s} & E_{3d_\sigma}-E & H_{d,\sigma} & H_{d,s'} \\ H_{\sigma,s} & H_{\sigma,d} & E_{5\sigma}-E & H_{\sigma,s'} \\ H_{s',s} & H_{s',d} & H_{s',\sigma} & E_{4s'}-E \end{vmatrix} = 0$$

Here the H_{ij}'s = $\langle\psi_i|H|\psi_j\rangle$ are the interaction energies between the orbitals indicated. E_{4s}, $E_{3d\sigma}$, $E_{4s'}$, and $E_{5\sigma}$ denote the energies of the corresponding orbitals in the absence of CO–metal ion bonding interaction. The energies of metal $3d_\sigma$ and 4s are known from variable photon energy PES and CIS studies, respectively, on clean CuCl and ZnO surfaces.[23] The energy of the CO 5σ level in the absence of bonding, $E_{5\sigma}$, is at 5.7 eV above the 4σ level. These E_i's are listed in Table II along with the values of the interaction energies H_{ij}'s obtained from these energies and the energy changes observed upon chemisorption (ΔE_i's in Table I).

Table II. Orbital and Interaction Energies (eV) for CO/M $3d^{10}$

matrix element	CO/CuCl	CO/ZnO
$H_{4s,5\sigma}$	4.8	3.1
$H_{3d,5\sigma}$	0.8	0.4
$H_{3d,2\pi^*}$	2.2	<2.2[a]
E_{M4s}	+2.5	+0.4
E_{M3d}	$-1.7(\sigma) - 2.7(\pi)$	−10.7
$E_{CO5\sigma}$	−7.6	−8.8
$E_{M4s'}$	−6.8	−7.5
$E_{CO2\pi^*}$	2.6	~3[b]

[a] Estimated upper limit (see text for details0. [b] Estimated energy based on inverse photoemission data for CO on metals and the results presented here for CO on CuCl.

The values in Table II enable one to quantitatively compare the contributions of σ bonding in these two d^{10} systems. σ bonding is found to be larger for Cu(I) than Zn(II) based on the larger destabilization of Cu 4s vs Zn 4s level upon CO adsorption from CIS studies. The energy change upon bonding is due to the M4s interaction with the CO 5σ and depends on the matrix element $H_{4s,5\sigma}$ and the energy difference ($E_{4s} - E_{5\sigma}$),

$$\Delta E_{4s,5\sigma} \simeq -(H_{4s,5\sigma})^2/(E_{4s} - E_{5\sigma})$$

where $\Delta E_{4s,5\sigma}$ is the energy of bonding only considering the CO 5σ interaction with the 4s orbital.[88] From Table II

$H_{4s,5\sigma}$ = 4.8 eV, $E_{4s} - E_{5\sigma}$ = 10.1 eV,
$\Delta E_{4s,5\sigma}$ = 2.3 eV for CO/CuCl

$H_{4s,5\sigma}$ = 3.1 eV, $E_{4s} - E_{5\sigma}$ = 9.2 eV,
$\Delta E_{4s,5\sigma}$ = 1.0 eV for CO/ZnO

Thus σ bonding is found to be stronger for Cu(I) not due to the energy difference of the interacting orbitals but due to the interaction energy $H_{4s,5\sigma}$ which is significantly larger for Cu(I) than for Zn(II). This matrix element is proportional to the overlap of the M4s and CO 5σ orbitals, $\langle\psi(4s)|\psi(5\sigma)\rangle$. Therefore the lower value of $H_{4s,5\sigma}$ for Zn(II) must originate from a reduced orbital overlap. This would derive from the higher effective nuclear charge for the Zn(II) ion which results in increased orbital contraction.

Calculation of the interaction energy for π back-bonding requires the energy of the CO $2\pi^*$ level. Before any bonding interaction, the CO $2\pi^*$ level is located above the $3d_\pi$ level (Figure 17a), with an energy gap Δ (=$E_{3d_\pi} - E_{2\pi^*}$). The matrix for bonding is

$$\begin{vmatrix} E_{3d_\pi}-E & H_{3d_\pi,2\pi^*} \\ H_{2\pi^*,3d_\pi} & E_{2\pi^*}-E \end{vmatrix} = 0$$

This interaction produces two molecular orbitals of which the bonding orbital is

$$\Psi_b = (\cos\theta)\psi_{3d} + (\sin\theta)\psi_{2\pi^*}$$

where ψ_{3d} and $\psi_{2\pi^*}$ are the wave functions of the orbitals on the metal and the CO and $\tan\theta = 2H_{3d\pi,2\pi^*}/\Delta$. Diagonalizing this matrix gives

$$\Delta E_{3d\pi} = ((\Delta^2 + 4H_{3d\pi,2\pi^*}{}^2)^{1/2} - \Delta)/2 \qquad (4)$$

where, as indicated in Figure 17a, $\Delta E_{3d\pi}$ is the energy change due to bonding and is known from PES studies (Table I). Because the energy position of the CO $2\pi^*$ and therefore Δ are not known, we cannot obtain $H_{3d\pi,2\pi^*}$ from $\Delta E_{3d\pi}$ directly, but we can estimate its value if we also include the C 1s core photoemission data in this analysis which should have approximately the same value for $H_{3d\pi,2\pi^*}$ in the core level final states. As shown in Figure 17b, upon ionization of a C 1s electron, final state relaxation occurs, shifting the CO $2\pi^*$ level below the metal 3d band by an energy U which corresponds to the energy of the electron-hole attraction.

(88) This will be close to the value of $-\Delta E_{4s}$ in Table I, which is determined by interaction with the CO 5σ, but the CO 5σ energy is also perturbed by its interaction with the 3d orbitals.

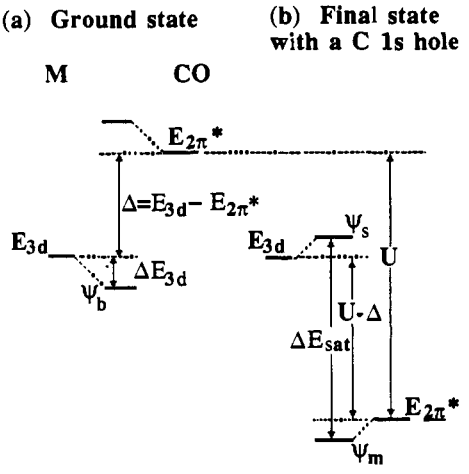

Figure 17. Energy-level diagram for the interaction between the M 3d and CO $2\pi^*$ orbitals: (a) the ground state for the CO/CuCl system and (b) two C 1s ionized final states. CO $2\pi^*$ is located above the Fermi level in the ground state but is relaxed to below the d levels by an energy U when a C 1s hole is created by photoionization. Two final states result from the interaction between the M 3d and CO $\underline{2\pi^*}$: screened and unscreened. For the screened final state, charge is transferred from the Cu 3d into the CO $\underline{2\pi^*}$ levels. The photoelectrons produced from the screened final state have higher kinetic energy (thus, lower binding energy) and correspond to the main peak (ψ_m). The photoelectrons from the unscreened state are at lower kinetic energy and correspond to the satellite peak (ψ_s) at higher binding energy, ΔE_{sat}.

The bonding interaction between the 3d and $\underline{2\pi^*}$ (which denotes the final state CO $2\pi^*$ level in the presence of a C 1s hole) leads to two different final states

$$\Psi_s = (\cos\theta')\psi_{3d} - (\sin\theta')\psi_{2\pi^*}$$

and

$$\Psi_m = (\sin\theta')\psi_{3d} + (\cos\theta')\psi_{2\pi^*}$$

with $\tan 2\theta' = 2H_{3d\pi,2\pi^*}/(\Delta - U)$. The two final states correspond to the main (ψ_m) and satellite (ψ_s) peaks in the C 1s PES spectrum with a main peak to satellite peak energy separation, ΔE_{sat}, of

$$\Delta E_{sat} = [(\Delta - U)^2 + 4(H_{3d\pi,2\pi^*})^2]^{1/2} \quad (5)$$

and an intensity ratio given by[89,90]

$$I_s/I_m = [(\sin\theta'\cos\theta - \cos\theta'\sin\theta)/(\cos\theta'\cos\theta + \sin\theta'\sin\theta)]^2 = \tan^2(\theta' - \theta) \quad (6)$$

Both ΔE_{sat} and I_s/I_m are known from the C 1s XPS data in Figure 10 and given in Table I. Thus for CO/CuCl, using $\Delta E_{3d\pi} = 0.8$ eV, $\Delta E_{sat} = 4.8$ eV, and $I_s/I_m = 0.5$ in eqs 4, 5, and 6 gives $H_{3d\pi,2\pi^*} = 2.2$ eV, $U = 7.4$ eV, and $\Delta = 5.3$ eV, which locates the CO $2\pi^*$ level at 2.6 eV above the Fermi level in the ground state in the absence of bonding. For CO/ZnO, measurable π back-bonding is not present based on the fact that satellite structure is not evident in the C 1s XPS spectrum and no π-polarized bonding shift in the Zn 3d region is observed.[91] We can however use eqs 4, 5, and 6 to estimate an upper limit for $\Delta E_{3d\pi}$ based on an upper limit of the I_s/I_m of ~10% allowed by the signal to noise of the ZnO data.[92] This gives a value of $H_{3d\pi,2\pi^*} < 3.5$ eV. However, $H_{3d\pi,2\pi^*}$ must be smaller than that of CO/Cu(I) due to orbital contraction (vide supra). Using the value of 2.2 eV obtained for CO/Cu(I) as a more reasonable upper limit for $H_{3d\pi,2\pi^*}$ (which corresponds to an I_s/I_m of ~5%) one obtains a $\Delta E_{3d\pi}$ of <0.3 eV. This upper limit for $\Delta E_{3d\pi}$ for CO/ZnO is much smaller than that observed for CO/CuCl (0.8 eV). This indicates that the weaker π back-bonding of CO/Zn(II) is mainly due to the much larger energy difference $E_{3d} - E_{2\pi}$ as compared to CO/CuCl (13.7 for CO/ZnO vs 5.3 eV for CO/CuCl). The 8.4 eV deeper binding energy of the d^{10} band in Zn(II) also derives from its higher effective nuclear charge relative to the Cu(I) ion.

Finally, these calculations provide insight into why σ donation dominates over π back-bonding for the CO/CuCl system. Table I gives a larger energy change due to σ bonding ($\Delta E_{M4s} = 2.0$ eV) relative to π bonding ($\Delta E_{M3d\pi} = 0.8$ eV), which is mainly due to the larger value of $H_{4s,5\sigma}$ vs $H_{3d,2\pi^*}$ (4.8 vs 2.2 eV) and relates to the increased overlap between Cu 4s and CO 5σ as compared to Cu 3d and CO $2\pi^*$ at the Cu(I)–CO bonding distance (vide infra). This dominance of σ bonding over π back-bonding has important consequences on the experimentally observed physical properties of the CO/CuCl system in that the surface dipole moment is observed to decrease and the C–O bond length is found to decrease, indicating a positively charged CO carbon and a net strengthened internal CO bond. Diagonalization of the above two matrices for σ and π bonding with the matrix elements in Table II gives an occupied CO 5σ wave function that has ~20% Cu 4s character and an occupied Cu 3d wave function with ~11% CO $2\pi^*$ character. Thus the electron charge donation from the CO 5σ to the metal is twice as great as that from the occupied Cu 3d into the CO $2\pi^*$ orbital. This large difference in σ vs π charge redistribution is particularly important in that one would expect that for the same amount of electron density change the π interaction would be more efficient than the σ interaction in charge transfer (as the 5σ electrons are on average closer to the Cu(I)) and in weakening the C–O bond (since the 5σ is only weakly antibonding due to configuration interaction).

The dependence of the strength of CO bonding on the effective nuclear charge is known from the following isoelectronic series of carbonyls: $[V(CO)_6^-$, $Cr(CO)_6$, and $Mn(CO)_6^+]$; $[Fe(CO)_4^{2-}$, $Co(CO)_4^-$, $Ni(CO)_4]$;[93] and $[Cr(CO)_5$, $Mn(CO)_5^+$, $Fe(CO)_5^{2+}]$.[94] In each series an increased effective nuclear charge results in an increase in the C–O vibrational stretching frequency, indicating weaker π back-bonding, due to the contraction of the metal d orbitals and thus a decrease in the overlap with the CO $2\pi^*$ orbital. The dependence of CO bonding on the effective nuclear charge is also demonstrated by CO adsorption behavior on a variety of transition-metal surfaces. Three types of chemisorption are observed: dissociative, strong nondissociative, and weak nondissociative. Dissociative adsorption is normally observed for transition metals to the left of the periodic table,[95-101] with heats of adsorption as high as 60–90 kcal/mol.[41] For this type of adsorption, π back-bonding is very strong, leading to C–O bond rupture. CO adsorption on group VIII transition metals is strong but nondissociative at or below room temperature, with heats of adsorption ranging from 28 kcal/mol on Ni to 45 kcal/mol on Pd.[40] CO chemisorption of this type always results in an increase in the work function and a decrease in the CO stretching frequency, demonstrating the dominance of π back-bonding. Weak nondissociative CO chemisorption occurs on group IB metals, with heats of adsorption of <15 kcal/mol.[40] Although π back-bonding still appears to dominate in the Cu(0)–CO bond (i.e. there is a small decrease in the CO stretching frequency (2096 vs 2143 cm^{-1} for

(89) Gerwirth, A. A.; Cohen, S.; Schugar, H.; Solomon, E. I. *Inorg. Chem.* **1987**, *26*, 1133.
(90) van der Lann, G.; Westra, C.; Haas, C.; Sawatsky, G. A. *Phys. Rev. B* **1981**, *23*, 4369.
(91) This region is however obscured by overlap of the CO 1π and 5σ peaks.
(92) This estimate is based on the assumptions that the CO $2\pi^*$ level in the absence of d_π–$2\pi^*$ bonding is located at ~3 eV above the Fermi level, which comes from inverse photoemission data for CO adsorbed on metal surfaces[61-65] as well as our result for CO/CuCl, and that the CO/Zn(II) oxide system has approximately the same value for the electron-hole attraction energy U as obtained for copper(II) chloride ($U = 8.9$ eV).[89]
(93) Elschenbroich, Ch.; Salzer, A. In *Organometallics*; VCH: New York, 1989; p 229.
(94) Hall, M. B.; Fenske, R. F. *Inorg. Chem.* **1972**, *11*, 1619.
(95) Broden, G.; Rhodin, T. N. *Solid State Commun.* **1976**, *18*, 105.
(96) Fukuda, Y.; Toyoshima, I. *Surf. Sci.* **1985**, *158*, 482.
(97) Benziger, J.; Madix, R. J. *Surf. Sci.* **1980**, *94*, 119.
(98) Hu, H.; Rabalais, J. W. *Surf. Sci.* **1981**, *107*, 376.
(99) Eastman, D. E. *Solid State Commun.* **1972**, *10*, 933.
(100) Fukuda, Y.; Lancaster, G. M.; Honda, F.; Rabalais, J. W. *J. Chem. Phys.* **1978**, *69*, 3447.
(101) Shincho, E.; Egawa, C.; Naito, S.; Tamaru, K. *Surf. Sci.* **1985**, *149*, 1.

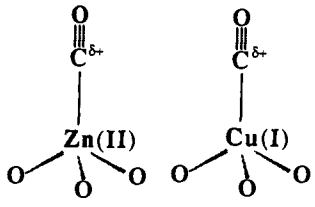

Figure 18. Models for the CO sites for ZnO and Cu/ZnO surfaces.

the gas phase)[40]), CO-covered Cu(0) shows a small decrease (−0.2 eV) in the surface work function[42] and CO adsorbed on Ag and Au surfaces both have higher ν_{C-O} (2182 and 2174 cm^{-1}).[102] Thus, on moving from left to right in the periodic table, the ability of a transition metal to donate charge into the CO $2\pi^*$ orbital decreases with increasing effective nuclear charge.

Data for CO bonding to d^{10} Ni(0) have also been included in Table I. Ni(0) has the lowest effective nuclear charge in this d^{10} series and should show the strongest σ bonding and π back-bonding, while Zn(II) should exhibit the weakest. This trend is reflected in the decreasing heats of adsorption from ΔH_0(CO/Ni(0)) = 28 kcal/mol, ΔH_0(CO/Cu(I)) = 23 kcal/mol, to ΔH_0(CO/Zn(II)) = 12 kcal/mol. The σ bonding in CO/Ni(0) is weaker than π bonding based on the positive $\Delta\phi$, ΔL_{C-O}, and a negative $\Delta\nu_{C-O}$ in Table I. This can be explained based on the model[103] that σ donation and π back-bonding are synergetic and optimal at different bonding distances. At longer distances, σ interaction dominates; at shorter distances π bonding becomes progressively more effective as does the repulsion between the CO 5σ electrons and the metal core electrons, both of which favor π bonding. For CO/Ni(100) the Ni–C distance is ~1.7 Å as determined by three-dimentional LEED.[104] For CO/Cu(I), crystallographic studies on Cu(I) carbonyls give a longer Cu(I)–C distance of ~1.8 Å,[44] which tends to form more dominant σ bonding. Additionally the positive charge on Cu(I) would tend to reduce σ repulsion. These factors lead to the net bonding description for CO/CuCl: π bonding with intermediate strength and weaker than σ bonding. For CO/ZnO, π interaction is negligible and the σ bonding weak based on the relatively long Zn–C distance (which is estimated to be ~2 Å from covalent radii).

Thus, the high effective nuclear charge of d^{10} ions appears to play a key role in defining the nature of CO bonding to these ions: Zn(II) has a high effective nuclear charge (and thus very contracted valence orbitals) and shows weak σ bonding with no π back-bonding; Cu(I) has lower nuclear charge and thus stronger σ bonding which still dominates over π back-bonding, resulting in a net charge transfer to the surface and in a strengthened CO bond. These bonding properties would appear to contribute strongly to the role of d^{10} ions in activating CO for methanol synthesis.

B. d^{10} Electronic Structure Contributions to CO Activation. There has been much discussion in the heterogeneous and homogeneous catalysis, theoretical and surface chemistry literature concerning the nature of the active sites, the small molecule species involved, and the mechanism of methanol synthesis from CO and H_2.[14,17,105-118] Our studies[7] of CO binding to different copper

Scheme II

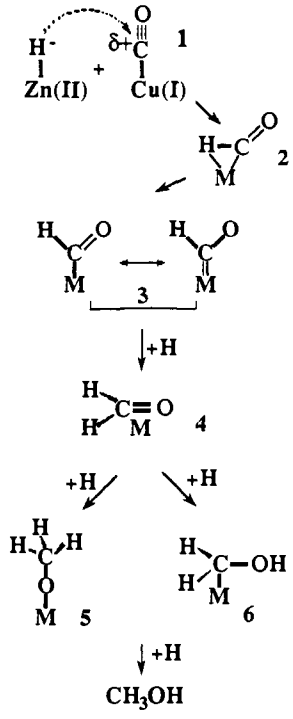

sites on different single-crystal surfaces of ZnO, combined with studies on the catalysts[14] indicating that the high-affinity CO binding sites correlate with reactivity, lead to the model for the copper site promoting CO activation shown in Figure 18. As with Zn(II), Cu(I) is in a coordinatively unsaturated tetrahedral C_{3v} site, and the studies presented here enable us to use a comparison of CO binding to these two related centers to probe for electronic structure differences which correlate with the differences in catalysis.

Both Cu(I) and Zn(II) surface sites appear to be particularly suited for selectively reducing CO to methanol since we have found the CO bond to be strengthened upon chemisorption to both sites consistent with the fact that the bond must be maintained in product formation. In addition, chemisorption on both coordinatively unsaturated Zn(II) and Cu(I) sites leads to net positive charge on the carbon which would activate CO toward nucleophilic attack by hydride which is present on ZnO surfaces as a result of the heterolytic dissociation of dihydrogen. Both properties derive from the fact that CO binding to both Cu(I) and Zn(II) is dominated by σ donation which transfers negative charge to the metal ion and removes electron density from the weakly antibonding (with respect to the CO bond) 5σ moleculr orbital. These results are consistent with the organometallic literture which finds that for the reaction of metal carbonyls with metal hydrides there is a threshold value of the CO force constant above which back-bonding is weak and nucleophilic attack on CO occurs.[119-121]

On a more quantitative level we have found that both σ donation and π back-bonding are significantly stronger for CO binding to Cu(I) than Zn(II), which leads to a stronger M–CO surface bond and hence a factor of 2 increase in the heat of adsorption for CO binding. This would raise the concentration of surface-bound CO

(102) Sheppard, N.; Nguyen, T. T. *Adv. Infrared Raman Spectrosc.* **1978**, *5*, 67 and references therein.
(103) Blomberg, M. R. A.; Brandemark, Ulf. B.; Siegbahn, Per. E. M.; Mathisen, K. B.; Karlstrom, G. *J. Phys. Chem.* **1985**, *89*, 2171.
(104) Passler, M.; Ignatiev, A.; Jona, F.; Jepsen, D. W.; Marcus, P. M. *Phys. Rev. Lett.* **1979**, *43*, 360.
(105) Kung, H. H. In *Transition Metal Oxides: Surface Chemistry and Catalysis*; Elsevier: New York, 1989; p 227.
(106) Collman, J. P.; Jegedus, L. S.; Norton, J. R.; Finke, R. G. In *Principles and Applications of Organotransition Metal Chemistry*; University Science Books, 1987; pp 1ff and references therein.
(107) Haggin, J. *C&E News* **1989**, *8*, 25.
(108) Frost, J. C. *Nature* **1988**, *334*, 577.
(109) Lee, G. v. d.; Ponec, V. *Catal. Rev.-Sci. Eng.* **1987**, *29*, 183.
(110) Poels, E. K.; Ponec, V. *Catalysis* **1983**, *7*, 196.
(111) Eisenberg, R.; Hendriksen, D. E. *Adv. Catal.* **1979**, *28*, 79.
(112) Ghiotti, G.; Boccuzzi, F. *Catal. Rev.-Sci. Eng.* **1987**, *29*, 151.
(113) Fakley, M. E.; Jennings, J. R.; Spencer, M. S. *J. Catal.* **1989**, *118*, 483.
(114) Costa, L. C. *Catal. Rev.-Sci. Eng.* **1983**, *25*, 325.
(115) Fahey, D. R. *J. Am. Chem. Soc.* **1981**, *103*, 136.
(116) Muetterties, E. L.; Stein, J. *Chem. Rev.* **1979**, *79*, 479.
(117) Chichen, G. C.; Waugh, K. C. *J. Catal.* **1986**, *97*, 280.
(118) Parker, D. G.; Pearce, R.; Prest, D. W. *J. Chem. Soc., Chem. Commun.* **1982**, 1193.
(119) Dombek, B. D. *Organometallics* **1985**, *4*, 1707.
(120) Angelici, R. J. *Acc. Chem. Rev.* **1972**, *5*, 335.
(121) Darensbourg, D. J.; Froelich, J. A. *J. Am. Chem. Soc.* **1977**, *99*, 5940.

$$\pi_{d_{xz}} + \sigma_{H^-} - 5\sigma_{CO} + 2\pi^*_{CO}$$

Figure 19. Schematic diagram of the ligand wave function ($\sigma_{H^-} - 5\sigma_{CO} + 2\pi^*_{CO}$) and its interaction with the metal $\pi_{d_{xz}}$ orbital associated with species **2** involved in the formation of formyl in Scheme II.

on the Cu(I)-promoted catalyst and increase the reaction rate.

A significant result of this study is that we have been able to estimate the relative charge on the carbon for CO bound to Cu(I) vs Zn(II) and find the latter to be more positive ($\Delta Q = +0.1$ vs 0.14 in Table I). This indicates that the role of copper in promoting methanol synthesis by lowering the activation barrier for catalysis by approximately a factor of 2 (18 versus 30 kcal/mol for pure ZnO)[13] is not simply an electrostatic activation of the hydride attack in Scheme II (which is a modified version of the Costa[114,115] and Muetterties[116] mechanisms) but must relate to the stabilization of a subsequent transition state in the reaction. The rate-determining step in Scheme II is considered to be the generation of the formaldehyde complex **4** which is thermodynamically uphill.[106,115,118] The key difference we find in the bonding of CO to Cu(I) vs Zn(II) is the presence of some π back-bonding involving the Cu(I) 3d orbitals. Berke and Hoffmann[122] have considered the energies of the orbitals involved in the hydride migration reaction to form the formyl species in Scheme II which proceeds through species **2**. Formation of this species is calculated to involve an increase in the energy of the occupied hydride σ orbital, σ_{H^-}, due to its antibonding interaction with the CO 5σ and $2\pi^*$ levels. As shown in Figure 19 the participation of energetically accessible d orbitals will assist in this bonding interaction and lower the energy destabilization of the ($\sigma_{H^-} - 5\sigma_{CO} + 2\pi^*_{CO}$) orbital of species **2** in Scheme II. However, this will reciprocally increase the energy of the d_{xz} orbital participating in this bonding and since Cu(I) is a d^{10} ion, this orbital is fully occupied and the total energy of species **2** will not be lowered by d bonding. Thus, d_π back-bonding does not appear to play a significant role in the formation of formyl via species **2**. Alternatively the presence of d_π back-bonding into unoccupied π^* orbitals of the ligand will significantly stabilize this formyl level intermediate **3** and the η^2-bidentate formaldehyde species **4** bound to the Cu(I)-active site. In particular, d_π back-bonding should increase the carbene character present in intermediate **3** which would assist in proton attack to produce formaldehyde. While species **5** or **6** does not appear to be involved in the rate-determining step in methanol synthesis, Baetzold has calculated the methoxy species **5** to also be stabilized by bonding to Cu(I).[123] Thus Cu(I) appears to be well suited electronically for CO activation in methanol synthesis in that while σ donation dominates (in contrast to metals) the presence of some π bonding can stabilize key intermediates involved in formaldehyde formation.

In summary, dominant σ bonding coupled with appreciable π back-bonding, which is found for CO bonding to Cu(I), appears to be most appropriate for methanol catalysis. The strong σ donation of CO to the active center is required to maintain the C–O bond and to activate the CO carbon for nucleophilic attack by hydride, while π back-bonding is necessary for stabilizing possible intermediates related to the activation barrier for catalysis. CO/Zn(II) shows weak σ bonding and therefore Zn(II) will activate hydride attack leading to the formyl species. However, Zn(II) is not particularly efficient for methanol synthesis due to the low heat of adsorption and high activation barrier which appears to relate to the lack of π back-bonding in this $3d^{10}$ metal ion.

Acknowledgment. We thank Prof. J. C. Merle of Universite Louis Pasteur, France for providing the single crystal used in this study. We are grateful to Prof. R. M. Waymouth for useful discussions. This work is supported by the NSF-MRL Program through the Center for Materials Research at Stanford University. Support for the work done at Stanford Synchrotron Radiation Laboratory which is operated by the Department of Energy, Division of Chemical Sciences is gratefully acknowledged. P.M.J. would also like to acknowledge the IBM Corporation for its financial support.

Registry No. CO, 630-08-0; CH_3OH, 67-56-1; Cu, 7440-50-8; ZnO, 1314-13-2; CuCl, 7758-89-6.

(122) Berke; Hoffmann, R. *J. Am. Chem. Soc.* **1978**, *100*, 7224.

(123) Baetzold, R. C. *J. Phys. Chem.* **1985**, *89*, 4150.